Research Paper
Computational Methods for Differential Equations
http://cmde.tabrizu.ac.ir
Vol. *, No. *, *, pp. 1-20
DOI:10.22034/cmde.2026.70845.3540

An advanced block-based algorithm for fractional order modeling of financial crime population dynamics prediction

Hadis Azin, Yadollah Ordokhani*, and Alireza Hosseinian

Department of Mathematics, Faculty of Mathematical Sciences, Alzahra University, Tehran, Iran.

Abstract

Developing robust population-level models of financial crimes is critical for quantifying systemic vulnerabilities, predicting illicit network growth patterns, and designing preemptive regulatory interventions that account for the nonlinear dynamics of modern economic systems. This study introduces a novel high-order computational framework based on quadratic interpolation for resolving complex fractional-order financial crime population systems. The developed technique significantly advances numerical solution capabilities by achieving simultaneous improvements in computational efficiency and solution accuracy for non-local differential operators. Our methodological innovation reconstructs the traditional block-by-block paradigm through a decoupling strategy that preserves solution autonomy beyond the initialization phase. This adaptation retains the numerical stability advantages of classical block methods while systematically eliminating solution interdependencies that traditionally compromise computational performance. A comprehensive convergence analysis establishes that the proposed scheme attains a convergence rate of $\mathcal{O}(\vartheta^{3+\xi})$ with ϑ step length and ξ fractional order. The numerical implementation provides conclusive verification of our method's theoretical advantages and practical utility in operational modeling scenarios.

Keywords. Financial crime modeling, Multi-step method, Quadratic interpolation, Fractional calculus, Convergence analysis.
2010 Mathematics Subject Classification. 32E30; 26A33; 35L45.

1. Introduction

Financial crime has become a critical threat to global economic stability, with increasingly sophisticated techniques such as cyber-enabled fraud and money laundering undermining financial systems [19]. Effective detection and prevention require advanced analytical frameworks to mitigate risks and ensure regulatory compliance [11]. Agent-based modeling (ABM) enables the simulation of interactions among autonomous agents in complex financial systems, providing new insights into crime dynamics [10]. Décary-Hétu and Giommoni applied epidemiological models to darknet market transactions, drawing novel parallels between contagion processes and illicit trade [5]. More recently, machine learning has been shown to enhance traditional econometric models, offering unprecedented accuracy in predicting financial crime patterns [13, 26].

Modeling the population dynamics of financial crime offers a valuable lens for understanding the evolution and diffusion of illicit activities within economic systems. Becker introduced rational choice theory into crime analysis [3], later extended by Reuter and Kleiman through the first system dynamics models of illicit markets [27]. Morselli advanced the field with social network analysis, showing how network topology influences the resilience of criminal enterprises [24]. Building on these foundations, researchers have employed agent-based simulations and network theory to reveal hidden patterns in money laundering, fraud propagation, and criminal adaptation to regulatory measures [4]. More recently, interdisciplinary approaches combining behavioral economics and machine learning have enabled the prediction of emerging threats, equipping policymakers with dynamic tools for proactive intervention [6].

Received: 22 December 2025; Accepted: 17 May 2026.
* Corresponding author. Email: ordokhani@alzahra.ac.ir.

Fractional-order models extend classical approaches by incorporating memory effects and anomalous diffusion - phenomena intrinsic to financial crimes but overlooked by traditional integer-order formulations. This mathematical framework enables a more accurate representation of self-reinforcing criminal networks and delayed regulatory impacts, both of which contribute to the persistence of illicit activities. Let $\mathcal{N}(t)$ denote the total population at time t, partitioned into five subgroups: susceptible individuals $\mathcal{S}(t)$, financial criminals $\mathcal{C}(t)$, individuals under prosecution $\mathcal{U}(t)$, prisoners $\mathcal{J}(t)$, and rehabilitated or honest individuals $\mathcal{H}(t)$. Assuming demographic stationarity, the dynamics of these subpopulations are described by the following nonlinear fractional-order system of differential equations [21]:

$$\begin{cases} {}_c^0D_t^\xi \mathcal{S}(t) = \rho_1 - \rho_2 \mathcal{S}(t)\mathcal{C}(t) - \big(\rho_1 + \rho_3\big)\mathcal{S}(t), \\ {}_c^0D_t^\xi \mathcal{C}(t) = \rho_2 \mathcal{S}(t)\mathcal{C}(t) + \rho_4\big(1-\rho_3\big)\mathcal{J}(t) - \big(\rho_1 + \rho_3 + \rho_5\big)\mathcal{C}(t) + \rho_6\rho_7\mathcal{U}(t), \\ {}_c^0D_t^\xi \mathcal{U}(t) = \rho_5 \mathcal{C}(t) - \big(\rho_1 + \rho_7 + \rho_8\big)\mathcal{U}(t), \\ {}_c^0D_t^\xi \mathcal{J}(t) = \rho_8 \mathcal{U}(t) - \big(\rho_1 + \rho_4\big)\mathcal{J}(t), \\ {}_c^0D_t^\xi \mathcal{H}(t) = \rho_7\big(1-\rho_6\big)\mathcal{U}(t) + \rho_3\big(\mathcal{S}(t) + \mathcal{C}(t)\big) + \rho_3\rho_4\mathcal{J}(t) - \rho_1\mathcal{H}(t), \end{cases} \tag{1.1}$$

subject to initial conditions

$$\mathcal{S}(0) = \mathcal{S}_0, \quad \mathcal{C}(0) = \mathcal{C}_0, \quad \mathcal{U}(0) = \mathcal{U}_0, \quad \mathcal{J}(0) = \mathcal{J}_0, \quad \mathcal{H}(0) = \mathcal{H}_0, \tag{1.2}$$

in which ${}_c^0D_t^\xi$ representing the Caputo fractional derivative operator, where the differentiation order ξ satisfies $0 < \xi \leq 1$. The model parameters regulate the rates of transition between subpopulations. Specifically, ρ_1 governs the inflow and outflow dynamics of the susceptible group, while ρ_2 captures the influence exerted by criminals on susceptibles. The parameter ρ_3 represents the rate of conversion to honest individuals, and ρ_4 denotes the release rate from jail. Prosecution dynamics are characterized by ρ_5, the per capita rate of financial crime prosecution, together with ρ_6 and ρ_7, which describe discharge proportions and acquittal rates, respectively. Finally, ρ_8 determines the rate at which prosecuted individuals are transferred to jail.

The analytical solution of the fractional-order financial crime system (1.1) is highly complex, if not intractable, thereby necessitating the use of numerical methods to obtain approximate solutions. Various approaches have been proposed in this context. For instance, the system has been solved using the Gegenbauer wavelet collocation method [21] and the Newton polynomial method [30]. In its integer-order form, an iterative scheme based on forward and backward Runge-Kutta methods of fourth order has been applied [2]. Beyond these, a wide range of numerical techniques have been developed to address the challenges of fractional-order systems, including the Adomian decomposition method [23], the differential transform method [8], and the fractional Taylor series method [17], each providing semi-analytical solutions with notable accuracy and efficiency. Additionally, finite difference schemes [9] and Laplace transform-based algorithms [18] have been employed, particularly for multi-term and nonlinear systems, offering step-by-step approximations that respect the inherent nonlocality of fractional derivatives.

The block-by-block method, first introduced by Young [29] in connection with the product integration technique, employs numerical integration and is notable for being self-starting and for producing a block of solution values simultaneously [7]. Block-wise computational techniques in numerical analysis, which operate on grouped data segments, exhibit a range of distinct benefits. They are particularly effective for solving problems over large intervals, where many conventional numerical methods become inefficient or fail. The block-by-block method requires no additional starting procedure or auxiliary function [16]. Furthermore, it is flexible in implementation, offers improved stability properties, and is well-suited for problems involving memory effects, such as fractional-order differential equations.

The attractive features of the block-by-block method have drawn considerable attention from researchers, leading to its application across a wide range of problems. These include Volterra integral equations [14, 28], fractional differential equations [12], fractional relaxation-oscillation equations [31], multi-term fractional differential equations [16], fractional integro-differential equations [1], and nonlinear two-dimensional Volterra integral equations [22]. Moreover, two- and three-block versions of the method have been successfully employed for solving nonlinear Volterra integral equations of the second kind [20]. The method has also been combined with the Romberg quadrature rule to address fractional systems of nonlinear weakly singular integro-differential equations [1, 15].

In this work, the fractional model (1.1) is addressed by converting it into an equivalent integral formulation. The solution domain $[0, T]$ is divided into $2\mathcal{K}$ uniformly spaced segments, enabling the discretization of the unknown

functions at each nodal point. Within the initial sub-interval $[0, t_1]$, quadratic interpolation is applied, and the resulting approximation is incorporated into the integral equation, forming the foundational problem of the system. This methodology is systematically extended to subsequent sub-intervals $[t_j, t_{j+1}]$ for $j = 1, 2, \cdots, 2\mathcal{K}-1$. Employing a quadratic Lagrange polynomial framework ultimately yields a complete system of equations that accurately represents the initial fractional problem.

The organization of this paper proceeds as follows: Section 2 introduces fundamental concepts and theoretical foundations of fractional calculus. Section 3 details the numerical methodology adopted for this investigation. A rigorous convergence analysis with examining the ∞-norm, is developed in section 4. Section 5 demonstrates computational experiments and interprets the resultant data. The study culminates in section 6 with concluding remarks that synthesize key discoveries and their broader significance.

2. Essential concepts of fractional calculus

This section establishes the mathematical foundation for subsequent algorithmic development by formalizing key fractional operator definitions and their fundamental characteristics. These constitutive elements provide the necessary theoretical infrastructure for our computational framework.

Definition 2.1. ([25]) Given a continuous function $z(t)$ on $t \in [a_1, a_2]$ and positive constant μ, the μ-th order fractional integral in the Riemann-Liouville sense is expressed as:

$$ {}^{a_1}_{RL}I^{\mu}_t z(t) = \frac{1}{\Gamma(\mu)} \int_{a_1}^{t} (t-w)^{\mu-1} z(w)\, dw. \tag{2.1} $$

Lemma 2.2. *([25]) Consider the power function space $\{(t-a_1)^i \mid i \geq 0\}$. The μ-order Riemann-Liouville fractional integral operator with $\mu > 0$ yields the following analytical expression:*

$$ {}^{a_1}_{RL}I^{\mu}_t (t-a_1)^i = \frac{\Gamma(i+1)}{\Gamma(i+1+\mu)} (t-a_1)^{i+\mu}. \tag{2.2} $$

Definition 2.3. ([25]) For a continuously differentiable real-valued function $z : [a_1, a_2] \longrightarrow \mathbb{R}$ and fractional exponent $\mu \in (0, 1]$, the Caputo fractional derivative (left-sided Caputo derivative) is defined by the expression:

$$ {}^{a_1}_{c}D^{\mu}_t z(t) = \begin{cases} \dfrac{1}{\Gamma(1-\mu)} \displaystyle\int_{a_1}^{t} (t-w)^{-\mu} z'(w) dw, & 0 < \mu < 1, \\ z'(t), & \mu = 1. \end{cases} \tag{2.3} $$

Lemma 2.4. *([25]) For integer $m \geq 1$ and fractional order $m-1 < \mu \leq m$, the fundamental compositional relationship between the Riemann-Liouville integral and Caputo differential operators for the function $z(t)$ in $[a_1, a_2]$ is given by:*

$$ {}^{a_1}_{RL}I^{\mu}_t \left({}^{a_1}_{c}D^{\mu}_t z(t) \right) = z(t) - \sum_{j=0}^{m-1} \frac{z^{(j)}(a_1)}{\Gamma(j+1)} (t-a_1)^j. \tag{2.4} $$

3. High-order block-by-block strategy

This section introduces an efficient multi-step numerical framework for addressing problem (1.1). Through systematic application of Riemann-Liouville integration operators coupled with Lemma 2.4, we derive the following equivalent formulation:

$$ \begin{aligned} \mathcal{S}(t) &= \mathcal{S}_0 + {}^{0}_{RL}I^{\xi}_t \Big(\mathcal{F}_1\big(t, \mathcal{S}(t), \mathcal{C}(t), \mathcal{U}(t), \mathcal{J}(t), \mathcal{H}(t)\big) \Big) \\ &= \mathcal{S}_0 + \frac{1}{\Gamma(\xi)} \int_0^t (t-w)^{\xi-1} \mathcal{F}_1\big(w, \mathcal{S}(w), \mathcal{C}(w), \mathcal{U}(w), \mathcal{J}(w), \mathcal{H}(w)\big) dw, \end{aligned} \tag{3.1} $$

$$ \mathcal{C}(t) = \mathcal{C}_0 + {}^{0}_{RL}I^{\xi}_t \Big(\mathcal{F}_2\big(t, \mathcal{S}(t), \mathcal{C}(t), \mathcal{U}(t), \mathcal{J}(t), \mathcal{H}(t)\big) \Big) $$

$$= \mathcal{C}_0 + \frac{1}{\Gamma(\xi)} \int_0^t (t-w)^{\xi-1} \mathcal{F}_2\big(w, \mathcal{S}(w), \mathcal{C}(w), \mathcal{U}(w), \mathcal{J}(w), \mathcal{H}(w)\big) dw, \tag{3.2}$$

$$\begin{aligned} \mathcal{U}(t) &= \mathcal{U}_0 + {}^{0}_{RL}I^{\xi}_{t}\Big(\mathcal{F}_3\big(t, \mathcal{S}(t), \mathcal{C}(t), \mathcal{U}(t), \mathcal{J}(t), \mathcal{H}(t)\big)\Big) \\ &= \mathcal{U}_0 + \frac{1}{\Gamma(\xi)} \int_0^t (t-w)^{\xi-1} \mathcal{F}_3\big(w, \mathcal{S}(w), \mathcal{C}(w), \mathcal{U}(w), \mathcal{J}(w), \mathcal{H}(w)\big) dw, \end{aligned} \tag{3.3}$$

$$\begin{aligned} \mathcal{J}(t) &= \mathcal{J}_0 + {}^{0}_{RL}I^{\xi}_{t}\Big(\mathcal{F}_4\big(t, \mathcal{S}(t), \mathcal{C}(t), \mathcal{U}(t), \mathcal{J}(t), \mathcal{H}(t)\big)\Big) \\ &= \mathcal{J}_0 + \frac{1}{\Gamma(\xi)} \int_0^t (t-w)^{\xi-1} \mathcal{F}_4\big(w, \mathcal{S}(w), \mathcal{C}(w), \mathcal{U}(w), \mathcal{J}(w), \mathcal{H}(w)\big) dw, \end{aligned} \tag{3.4}$$

and

$$\begin{aligned} \mathcal{H}(t) &= \mathcal{H}_0 + {}^{0}_{RL}I^{\xi}_{t}\Big(\mathcal{F}_5\big(t, \mathcal{S}(t), \mathcal{C}(t), \mathcal{U}(t), \mathcal{J}(t), \mathcal{H}(t)\big)\Big) \\ &= \mathcal{H}_0 + \frac{1}{\Gamma(\xi)} \int_0^t (t-w)^{\xi-1} \mathcal{F}_5\big(t, \mathcal{S}(t), \mathcal{C}(t), \mathcal{U}(t), \mathcal{J}(t), \mathcal{H}(t)\big) dw, \end{aligned} \tag{3.5}$$

in which

$$\begin{cases} \mathcal{F}_1\big(t, \mathcal{S}(t), \mathcal{C}(t), \mathcal{U}(t), \mathcal{J}(t), \mathcal{H}(t)\big) = \rho_1 - \rho_2 \mathcal{S}(t)\mathcal{C}(t) - \big(\rho_1 + \rho_3\big)\mathcal{S}(t), \\ \mathcal{F}_2\big(t, \mathcal{S}(t), \mathcal{C}(t), \mathcal{U}(t), \mathcal{J}(t), \mathcal{H}(t)\big) = \rho_2 \mathcal{S}(t)\mathcal{C}(t) + \rho_4\big(1-\rho_3\big)\mathcal{J}(t) - \big(\rho_1 + \rho_3 + \rho_5\big)\mathcal{C}(t) + \rho_6\rho_7\mathcal{U}(t), \\ \mathcal{F}_3\big(t, \mathcal{S}(t), \mathcal{C}(t), \mathcal{U}(t), \mathcal{J}(t), \mathcal{H}(t)\big) = \rho_5 \mathcal{C}(t) - \big(\rho_1 + \rho_7 + \rho_8\big)\mathcal{U}(t), \\ \mathcal{F}_4\big(t, \mathcal{S}(t), \mathcal{C}(t), \mathcal{U}(t), \mathcal{J}(t), \mathcal{H}(t)\big) = \rho_8 \mathcal{U}(t) - \big(\rho_1 + \rho_4\big)\mathcal{J}(t), \\ \mathcal{F}_5\big(t, \mathcal{S}(t), \mathcal{C}(t), \mathcal{U}(t), \mathcal{J}(t), \mathcal{H}(t)\big) = \rho_7\big(1-\rho_6\big)\mathcal{U}(t) + \rho_3\big(\mathcal{S}(t) + \mathcal{C}(t)\big) + \rho_3\rho_4\mathcal{J}(t) - \rho_1\mathcal{H}(t). \end{cases} \tag{3.6}$$

To develop a discrete numerical scheme, we divide the temporal domain $[0, T]$ into $2\mathcal{K}$ uniformly spaced nodes t_j, where $t_j = j\vartheta$ with step size $\vartheta = \dfrac{T}{2\mathcal{K}}$ for $j = 0, 1, 2, \ldots, 2\mathcal{K}$. The numerical solution is first approximated at the initial nodal points. Employing quadratic interpolation over the sub-interval $[0, t_1]$, we derive an approximate representation of the integrand functions $\mathcal{F}_k$ for $k = 1, 2, 3, 4, 5$ in relations (3.1)-(3.5), yielding the following discretized form:

$$\mathcal{F}_k\big(t, \mathcal{S}(t), \mathcal{C}(t), \mathcal{U}(t), \mathcal{J}(t), \mathcal{H}(t)\big)\Big|_{[0,t_1]} \simeq \frac{2(t-t_{\frac{1}{2}})(t-t_1)}{\vartheta^2}\mathcal{F}_k^0 + \frac{-4(t-t_0)(t-t_1)}{\vartheta^2}\mathcal{F}_k^{\frac{1}{2}} + \frac{2(t-t_0)(t-t_{\frac{1}{2}})}{\vartheta^2}\mathcal{F}_k^1, \tag{3.7}$$

in which $\mathcal{F}_k^r = \mathcal{F}_k\big(t_r, \mathcal{S}(t_r), \mathcal{C}(t_r), \mathcal{U}(t_r), \mathcal{J}(t_r), \mathcal{H}(t_r)\big)$ and $t_{\frac{1}{2}} = \frac{\vartheta}{2}$. The quadratic interpolation scheme is subsequently applied to estimate $\mathcal{F}_k^{\frac{1}{2}}$, producing the following approximation:

$$\mathcal{F}_k^{\frac{1}{2}} \simeq \frac{3}{8}\mathcal{F}_k^0 + \frac{3}{4}\mathcal{F}_k^1 - \frac{1}{8}\mathcal{F}_k^2. \tag{3.8}$$

The nodal approximation of $\mathcal{S}(t_1)$, $\mathcal{C}(t_1)$, $\mathcal{U}(t_1)$, $\mathcal{J}(t_1)$ and $\mathcal{H}(t_1)$ is derived through substitution of (3.7)-(3.8) into (3.1)-(3.5) and applying Lemma 2.2, yielding:

$$\begin{cases} \mathcal{S}(t_1) \simeq \mathcal{S}_0 + \varepsilon_0^{(1)}\mathcal{F}_1^0 + \varepsilon_1^{(1)}\mathcal{F}_1^1 + \varepsilon_2^{(1)}\mathcal{F}_1^2, \\ \mathcal{C}(t_1) \simeq \mathcal{C}_0 + \varepsilon_0^{(1)}\mathcal{F}_2^0 + \varepsilon_1^{(1)}\mathcal{F}_2^1 + \varepsilon_2^{(1)}\mathcal{F}_2^2, \\ \mathcal{U}(t_1) \simeq \mathcal{U}_0 + \varepsilon_0^{(1)}\mathcal{F}_3^0 + \varepsilon_1^{(1)}\mathcal{F}_3^1 + \varepsilon_2^{(1)}\mathcal{F}_3^2, \\ \mathcal{J}(t_1) \simeq \mathcal{J}_0 + \varepsilon_0^{(1)}\mathcal{F}_4^0 + \varepsilon_1^{(1)}\mathcal{F}_4^1 + \varepsilon_2^{(1)}\mathcal{F}_4^2, \\ \mathcal{H}(t_1) \simeq \mathcal{H}_0 + \varepsilon_0^{(1)}\mathcal{F}_5^0 + \varepsilon_1^{(1)}\mathcal{F}_5^1 + \varepsilon_2^{(1)}\mathcal{F}_5^2, \end{cases} \tag{3.9}$$

in which

$$\begin{aligned}\varepsilon_0^{(1)} &= \frac{1}{\Gamma(\xi)}\int_0^{t_1}(t_1-w)^{\xi-1}\left(\frac{2(w-t_{\frac{1}{2}})(w-t_1)}{\vartheta^2}\right)dw + \frac{3}{8\Gamma(\xi)}\int_0^{t_1}(t_1-w)^{\xi-1}\left(\frac{-4(w-t_0)(w-t_1)}{\vartheta^2}\right)dw\\ &= \frac{2}{\vartheta^2}\left({}^{0}_{RL}I^{\xi}_{t_1}t^2-\left(t_{\frac{1}{2}}+t_1\right){}^{0}_{RL}I^{\xi}_{t_1}t+t_{\frac{1}{2}}t_1\,{}^{0}_{RL}I^{\xi}_{t_1}1\right)-\frac{3}{2\vartheta^2}\left({}^{0}_{RL}I^{\xi}_{t_1}t^2-\left(t_0+t_1\right){}^{0}_{RL}I^{\xi}_{t_1}t+t_0t_1\,{}^{0}_{RL}I^{\xi}_{t_1}1\right)\\ &= \frac{2}{\vartheta^2}\left(\frac{\Gamma(3)}{\Gamma(3+\xi)}t_1^{2+\xi}-\left(t_{\frac{1}{2}}+t_1\right)\frac{\Gamma(2)}{\Gamma(2+\xi)}t_1^{1+\xi}+\frac{t_{\frac{1}{2}}t_1}{\Gamma(1+\xi)}t_1^{\xi}\right)\\ &\quad-\frac{3}{2\vartheta^2}\left(\frac{\Gamma(3)}{\Gamma(3+\xi)}t_1^{2+\xi}-\left(t_0+t_1\right)\frac{\Gamma(2)}{\Gamma(2+\xi)}t_1^{1+\xi}+\frac{t_0t_1}{\Gamma(1+\xi)}t_1^{\xi}\right),\end{aligned}\tag{3.10}$$

$$\begin{aligned}\varepsilon_1^{(1)} &= \frac{3}{4\Gamma(\xi)}\int_0^{t_1}(t_1-w)^{\xi-1}\left(\frac{-4(w-t_0)(w-t_1)}{\vartheta^2}\right)dw + \frac{1}{\Gamma(\xi)}\int_0^{t_1}(t_1-w)^{\xi-1}\left(\frac{2(w-t_0)(w-t_{\frac{1}{2}})}{\vartheta^2}\right)dw\\ &= \frac{-3}{\vartheta^2}\left({}^{0}_{RL}I^{\xi}_{t_1}t^2-\left(t_0+t_1\right){}^{0}_{RL}I^{\xi}_{t_1}t+t_0t_1\,{}^{0}_{RL}I^{\xi}_{t_1}1\right)+\frac{2}{\vartheta^2}\left({}^{0}_{RL}I^{\xi}_{t_1}t^2-\left(t_0+t_{\frac{1}{2}}\right){}^{0}_{RL}I^{\xi}_{t_1}t+t_0t_{\frac{1}{2}}\,{}^{0}_{RL}I^{\xi}_{t_1}1\right)\\ &= \frac{-3}{\vartheta^2}\left(\frac{\Gamma(3)}{\Gamma(3+\xi)}t_1^{2+\xi}-\left(t_0+t_1\right)\frac{\Gamma(2)}{\Gamma(2+\xi)}t_1^{1+\xi}+\frac{t_0t_1}{\Gamma(1+\xi)}t_1^{\xi}\right)\\ &\quad+\frac{2}{\vartheta^2}\left(\frac{\Gamma(3)}{\Gamma(3+\xi)}t_1^{2+\xi}-\left(t_0+t_{\frac{1}{2}}\right)\frac{\Gamma(2)}{\Gamma(2+\xi)}t_1^{1+\xi}+\frac{t_0t_{\frac{1}{2}}}{\Gamma(1+\xi)}t_1^{\xi}\right),\end{aligned}\tag{3.11}$$

and

$$\begin{aligned}\varepsilon_2^{(1)} &= \frac{-1}{8\Gamma(\xi)}\int_0^{t_1}(t_1-w)^{\xi-1}\left(\frac{-4(w-t_0)(w-t_1)}{\vartheta^2}\right)dw = \frac{1}{2\vartheta^2}\left({}^{0}_{RL}I^{\xi}_{t_1}t^2-\left(t_0+t_1\right){}^{0}_{RL}I^{\xi}_{t_1}t+t_0t_1\,{}^{0}_{RL}I^{\xi}_{t_1}1\right)\\ &= \frac{1}{2\vartheta^2}\left(\frac{\Gamma(3)}{\Gamma(3+\xi)}t_1^{2+\xi}-\left(t_0+t_1\right)\frac{\Gamma(2)}{\Gamma(2+\xi)}t_1^{1+\xi}+\frac{t_0t_1}{\Gamma(1+\xi)}t_1^{\xi}\right).\end{aligned}\tag{3.12}$$

Following the analogous procedure, the approximation the unknown functions in problem (3.1) to (3.5) in point t_2 is determined by first applying quadratic interpolation over $[0,t_2]$ to approximation the function $\mathcal{F}_k\big(t,\mathcal{S}(t),\mathcal{C}(t),\mathcal{U}(t),\mathcal{J}(t),\mathcal{H}(t)\big)$ with $1\le k\le 5$, obtaining:

$$\mathcal{F}_k\big(t,\mathcal{S}(t),\mathcal{C}(t),\mathcal{U}(t),\mathcal{J}(t),\mathcal{H}(t)\big)\Big|_{[0,t_2]} \simeq \frac{(t-t_1)(t-t_2)}{2\vartheta^2}\mathcal{F}_k^0+\frac{-(t-t_0)(t-t_2)}{\vartheta^2}\mathcal{F}_k^1+\frac{(t-t_0)(t-t_1)}{2\vartheta^2}\mathcal{F}_k^2,\tag{3.13}$$

and producing the following computational outcomes as:

$$\begin{cases}\mathcal{S}(t_2)\simeq\mathcal{S}_0+\varepsilon_0^{(2)}\mathcal{F}_1^0+\varepsilon_1^{(2)}\mathcal{F}_1^1+\varepsilon_2^{(2)}\mathcal{F}_1^2,\\ \mathcal{C}(t_2)\simeq\mathcal{C}_0+\varepsilon_0^{(2)}\mathcal{F}_2^0+\varepsilon_1^{(2)}\mathcal{F}_2^1+\varepsilon_2^{(2)}\mathcal{F}_2^2,\\ \mathcal{U}(t_2)\simeq\mathcal{U}_0+\varepsilon_0^{(2)}\mathcal{F}_3^0+\varepsilon_1^{(2)}\mathcal{F}_3^1+\varepsilon_2^{(2)}\mathcal{F}_3^2,\\ \mathcal{J}(t_2)\simeq\mathcal{J}_0+\varepsilon_0^{(2)}\mathcal{F}_4^0+\varepsilon_1^{(2)}\mathcal{F}_4^1+\varepsilon_2^{(2)}\mathcal{F}_4^2,\\ \mathcal{H}(t_2)\simeq\mathcal{H}_0+\varepsilon_0^{(2)}\mathcal{F}_5^0+\varepsilon_1^{(2)}\mathcal{F}_5^1+\varepsilon_2^{(2)}\mathcal{F}_5^2,\end{cases}\tag{3.14}$$

in which

$$\begin{aligned}\varepsilon_0^{(2)} &= \frac{1}{\Gamma(\xi)}\int_0^{t_2}(t_2-w)^{\xi-1}\left(\frac{(w-t_1)(w-t_2)}{2\vartheta^2}\right)dw = \frac{1}{2\vartheta^2}\left({}^{0}_{RL}I^{\xi}_{t_2}t^2-\left(t_1+t_2\right){}^{0}_{RL}I^{\xi}_{t_2}t+t_1t_2\,{}^{0}_{RL}I^{\xi}_{t_2}1\right)\\ &= \frac{1}{2\vartheta^2}\left(\frac{\Gamma(3)}{\Gamma(3+\xi)}t_2^{2+\xi}-\left(t_1+t_2\right)\frac{\Gamma(2)}{\Gamma(2+\xi)}t_2^{1+\xi}+\frac{t_1t_2}{\Gamma(1+\xi)}t_2^{\xi}\right),\end{aligned}\tag{3.15}$$

$$\varepsilon_1^{(2)} = \frac{-1}{\Gamma(\xi)}\int_0^{t_2}(t_2-w)^{\xi-1}\left(\frac{(w-t_0)(w-t_2)}{\vartheta^2}\right)dw = \frac{-1}{\vartheta^2}\left({}^{0}_{RL}I^{\xi}_{t_2}t^2-\left(t_0+t_2\right){}^{0}_{RL}I^{\xi}_{t_2}t+t_0t_2\,{}^{0}_{RL}I^{\xi}_{t_2}1\right)$$

$$= \frac{-1}{\vartheta^2}\left(\frac{\Gamma(3)}{\Gamma(3+\xi)}t_2^{2+\xi} - (t_0+t_2)\frac{\Gamma(2)}{\Gamma(2+\xi)}t_2^{1+\xi} + \frac{t_0t_2}{\Gamma(1+\xi)}t_2^{\xi}\right), \tag{3.16}$$

and

$$\begin{aligned}\varepsilon_2^{(2)} &= \frac{1}{\Gamma(\xi)}\int_0^{t_2}(t_2-w)^{\xi-1}\left(\frac{(w-t_0)(w-t_1)}{2\vartheta^2}\right)dw = \frac{1}{2\vartheta^2}\left({}_{RL}^{0}I_{t_2}^{\xi}t^2 - (t_0+t_1)\,{}_{RL}^{0}I_{t_2}^{\xi}t + t_0t_1\,{}_{RL}^{0}I_{t_2}^{\xi}1\right)\\ &= \frac{1}{2\vartheta^2}\left(\frac{\Gamma(3)}{\Gamma(3+\xi)}t_2^{2+\xi} - (t_0+t_1)\frac{\Gamma(2)}{\Gamma(2+\xi)}t_2^{1+\xi} + \frac{t_0t_1}{\Gamma(1+\xi)}t_2^{\xi}\right).\end{aligned} \tag{3.17}$$

Building upon the established discretization scheme, we now develop the computational framework for advancing the solution to subsequent time steps. The objective is to deriving estimates for the solution at the subsequent odd and even nodal points t_{2s+1} and t_{2s+2} , where $s = 1, 2, \ldots, \mathcal{K}-1$. By applying the interpolation methodology applied in earlier steps for $\mathcal{F}_k\big(t, \mathcal{S}(t), \mathcal{C}(t), \mathcal{U}(t), \mathcal{J}(t), \mathcal{H}(t)\big)$ on $[0, t_{2s+1}]$ and $[0, t_{2s+2}]$—leveraging quadratic polynomial approximation—we derive the following relations:

$$\begin{aligned}&\frac{1}{\Gamma(\xi)}\int_0^{t_{2s+1}}(t_{2s+1}-w)^{\xi-1}\mathcal{F}_k\big(w,\mathcal{S}(w),\mathcal{C}(w),\mathcal{U}(w),\mathcal{J}(w),\mathcal{H}(w)\big)dw\\ &= \frac{1}{\Gamma(\xi)}\int_0^{t_1}(t_{2s+1}-w)^{\xi-1}\mathcal{F}_k\big(w,\mathcal{S}(w),\mathcal{C}(w),\mathcal{U}(w),\mathcal{J}(w),\mathcal{H}(w)\big)dw\\ &+ \sum_{l=1}^{s}\frac{1}{\Gamma(\xi)}\int_{t_{2l-1}}^{t_{2l+1}}(t_{2s+1}-w)^{\xi-1}\mathcal{F}_k\big(w,\mathcal{S}(w),\mathcal{C}(w),\mathcal{U}(w),\mathcal{J}(w),\mathcal{H}(w)\big)dw\\ &\simeq \sigma_0^{(s)}\mathcal{F}_k^0 + \sigma_1^{(s)}\mathcal{F}_k^1 + \sigma_2^{(s)}\mathcal{F}_k^2 + \sum_{l=1}^{s}\sigma_{2l-1}^{(s)}\mathcal{F}_k^{2l-1} + \sigma_{2l}^{(s)}\mathcal{F}_k^{2l} + \sigma_{2l+1}^{(s)}\mathcal{F}_k^{2l+1},\end{aligned} \tag{3.18}$$

and

$$\begin{aligned}&\frac{1}{\Gamma(\xi)}\int_0^{t_{2s+2}}(t_{2s+2}-w)^{\xi-1}\mathcal{F}_k\big(w,\mathcal{S}(w),\mathcal{C}(w),\mathcal{U}(w),\mathcal{J}(w),\mathcal{H}(w)\big)dw\\ &= \sum_{q=0}^{s}\frac{1}{\Gamma(\xi)}\int_{t_{2q}}^{t_{2q+2}}(t_{2s+2}-w)^{\xi-1}\mathcal{F}_k\big(w,\mathcal{S}(w),\mathcal{C}(w),\mathcal{U}(w),\mathcal{J}(w),\mathcal{H}(w)\big)dw\\ &\simeq \sum_{q=0}^{s}\upsilon_{2q}^{(s)}\mathcal{F}_k^{2q} + \upsilon_{2q+1}^{(s)}\mathcal{F}_k^{2q+1} + \upsilon_{2q+2}^{(s)}\mathcal{F}_k^{2q+2},\end{aligned} \tag{3.19}$$

in which

$$\begin{aligned}\sigma_0^{(s)} &= \frac{1}{\Gamma(\xi)}\int_0^{t_1}(t_{2s+1}-w)^{\xi-1}\left(\frac{2(w-t_{\frac{1}{2}})(w-t_1)}{\vartheta^2}\right)dw\\ &+ \frac{3}{8\Gamma(\xi)}\int_0^{t_1}(t_{2s+1}-w)^{\xi-1}\left(\frac{-4(w-t_0)(w-t_1)}{\vartheta^2}\right)dw\\ &= \frac{2}{\vartheta^2}\Big(\mathcal{Q}_2\big(0,t_1,t_{2s+1}\big) - (t_{\frac{1}{2}}+t_1)\mathcal{Q}_1\big(0,t_1,t_{2s+1}\big) + t_{\frac{1}{2}}t_1\mathcal{Q}_0\big(0,t_1,t_{2s+1}\big)\Big)\\ &+ \frac{3}{8\vartheta^2}\Big(\mathcal{Q}_2\big(0,t_1,t_{2s+1}\big) - (t_0+t_1)\mathcal{Q}_1\big(0,t_1,t_{2s+1}\big) + t_0t_1\mathcal{Q}_0\big(0,t_1,t_{2s+1}\big)\Big),\end{aligned} \tag{3.20}$$

$$\begin{aligned}\sigma_1^{(s)} &= \frac{3}{4\Gamma(\xi)}\int_0^{t_1}(t_{2s+1}-w)^{\xi-1}\left(\frac{-4(w-t_0)(w-t_1)}{\vartheta^2}\right)dw\\ &+ \frac{1}{\Gamma(\xi)}\int_0^{t_1}(t_{2s+1}-w)^{\xi-1}\left(\frac{2(w-t_0)(w-t_{\frac{1}{2}})}{\vartheta^2}\right)dw\\ &= \frac{-3}{\vartheta^2}\Big(\mathcal{Q}_2\big(0,t_1,t_{2s+1}\big) - (t_0+t_1)\mathcal{Q}_1\big(0,t_1,t_{2s+1}\big) + t_0t_1\mathcal{Q}_0\big(0,t_1,t_{2s+1}\big)\Big)\end{aligned} \tag{3.21}$$

$$+\frac{2}{\vartheta^2}\Big(\mathcal{Q}_2(0,t_1,t_{2s+1})-(t_0+t_{\frac{1}{2}})\mathcal{Q}_1(0,t_1,t_{2s+1})+t_0t_{\frac{1}{2}}\mathcal{Q}_0(0,t_1,t_{2s+1})\Big), \tag{3.22}$$

$$\begin{aligned}\sigma_2^{(s)}&=\frac{-1}{8\Gamma(\xi)}\int_0^{t_1}(t_{2s+1}-w)^{\xi-1}\Big(\frac{-4(w-t_0)(w-t_1)}{\vartheta^2}\Big)dw\\&=\frac{1}{2\vartheta^2}\Big(\mathcal{Q}_2(0,t_1,t_{2s+1})-(t_0+t_1)\mathcal{Q}_1(0,t_1,t_{2s+1})+t_0t_1\mathcal{Q}_0(0,t_1,t_{2s+1})\Big),\end{aligned} \tag{3.23}$$

$$\begin{aligned}\sigma_{2l-1}^{(s)}&=\frac{1}{\Gamma(\xi)}\int_{t_{2l-1}}^{t_{2l+1}}(t_{2s+1}-w)^{\xi-1}\Big(\frac{(w-t_{2l})(w-t_{2l+1})}{2\vartheta^2}\Big)dw\\&=\frac{1}{2\vartheta^2}\Big(\mathcal{Q}_2(t_{2l-1},t_{2l+1},t_{2s+1})-(t_{2l}+t_{2l+1})\mathcal{Q}_1(t_{2l-1},t_{2l+1},t_{2s+1})+t_{2l}t_{2l+1}\mathcal{Q}_0(t_{2l-1},t_{2l+1},t_{2s+1})\Big),\end{aligned} \tag{3.24}$$

$$\begin{aligned}\sigma_{2l}^{(s)}&=\frac{1}{\Gamma(\xi)}\int_{t_{2l-1}}^{t_{2l+1}}(t_{2s+1}-w)^{\xi-1}\Big(\frac{(w-t_{2l-1})(w-t_{2l+1})}{-\vartheta^2}\Big)dw\\&=\frac{-1}{\vartheta^2}\Big(\mathcal{Q}_2(t_{2l-1},t_{2l+1},t_{2s+1})-(t_{2l-1}+t_{2l+1})\mathcal{Q}_1(t_{2l-1},t_{2l+1},t_{2s+1})+t_{2l-1}t_{2l+1}\mathcal{Q}_0(t_{2l-1},t_{2l+1},t_{2s+1})\Big),\end{aligned} \tag{3.25}$$

$$\begin{aligned}\sigma_{2l+1}^{(s)}&=\frac{1}{\Gamma(\xi)}\int_{t_{2l-1}}^{t_{2l+1}}(t_{2s+1}-w)^{\xi-1}\Big(\frac{(w-t_{2l})(w-t_{2l-1})}{2\vartheta^2}\Big)dw\\&=\frac{1}{2\vartheta^2}\Big(\mathcal{Q}_2(t_{2l-1},t_{2l+1},t_{2s+1})-(t_{2l}+t_{2l-1})\mathcal{Q}_1(t_{2l-1},t_{2l+1},t_{2s+1})+t_{2l}t_{2l-1}\mathcal{Q}_0(t_{2l-1},t_{2l+1},t_{2s+1})\Big),\end{aligned} \tag{3.26}$$

and

$$\begin{aligned}\upsilon_{2q}^{(s)}&=\frac{1}{\Gamma(\xi)}\int_{t_{2q}}^{t_{2q+2}}(t_{2s+2}-w)^{\xi-1}\Big(\frac{(w-t_{2q+1})(w-t_{2q+2})}{2\vartheta^2}\Big)dw\\&=\frac{1}{2\vartheta^2}\Big(\mathcal{Q}_2(t_{2q},t_{2q+2},t_{2s+2})-(t_{2q+1}+t_{2q+2})\mathcal{Q}_1(t_{2q},t_{2q+2},t_{2s+2})+t_{2q+1}t_{2q+2}\mathcal{Q}_0(t_{2q},t_{2q+2},t_{2s+2})\Big),\end{aligned} \tag{3.27}$$

$$\begin{aligned}\upsilon_{2q+1}^{(s)}&=\frac{1}{\Gamma(\xi)}\int_{t_{2q}}^{t_{2q+2}}(t_{2s+2}-w)^{\xi-1}\Big(\frac{(w-t_{2q})(w-t_{2q+2})}{-\vartheta^2}\Big)dw\\&=\frac{-1}{\vartheta^2}\Big(\mathcal{Q}_2(t_{2q},t_{2q+2},t_{2s+2})-(t_{2q}+t_{2q+2})\mathcal{Q}_1(t_{2q},t_{2q+2},t_{2s+2})+t_{2q}t_{2q+2}\mathcal{Q}_0(t_{2q},t_{2q+2},t_{2s+2})\Big),\end{aligned} \tag{3.28}$$

$$\begin{aligned}\upsilon_{2q+2}^{(s)}&=\frac{1}{\Gamma(\xi)}\int_{t_{2q}}^{t_{2q+2}}(t_{2s+2}-w)^{\xi-1}\Big(\frac{(w-t_{2q})(w-t_{2q+2})}{2\vartheta^2}\Big)dw\\&=\frac{1}{2\vartheta^2}\Big(\mathcal{Q}_2(t_{2q},t_{2q+2},t_{2s+2})-(t_{2q}+t_{2q+2})\mathcal{Q}_1(t_{2q},t_{2q+2},t_{2s+2})+t_{2q}t_{2q+2}\mathcal{Q}_0(t_{2q},t_{2q+2},t_{2s+2})\Big),\end{aligned} \tag{3.29}$$

where the integral terms appearing in relation (3.20)-(3.29) exhibit $\frac{1}{\Gamma(\xi)}\int_a^b(c-w)^{\xi-1}w^p dw$ for $p=0,1,2$ with the constants a,b,c and are evaluated analytically through integration by parts as follows:

$$\begin{aligned}\mathcal{Q}_2(a,b,c)&=\frac{1}{\Gamma(\xi)}\int_a^b(c-w)^{\xi-1}w^2dw=-\frac{(c-b)^\xi b^2}{\Gamma(\xi+1)}+\frac{(c-a)^\xi a^2}{\Gamma(\xi+1)}-\frac{2(c-b)^{\xi+1}b}{\Gamma(\xi+2)}\\&\quad+\frac{2(c-a)^{\xi+1}a}{\Gamma(\xi+2)}-\frac{2(c-b)^{\xi+2}}{\Gamma(\xi+3)}+\frac{2(c-a)^{\xi+2}}{\Gamma(\xi+3)},\end{aligned} \tag{3.30}$$

and

$$\mathcal{Q}_1(a,b,c)=\frac{1}{\Gamma(\xi)}\int_a^b(c-w)^{\xi-1}wdw=-\frac{(c-b)^\xi b}{\Gamma(\xi+1)}+\frac{(c-a)^\xi a}{\Gamma(\xi+1)}-\frac{(c-b)^{\xi+1}}{\Gamma(\xi+2)}+\frac{(c-a)^{\xi+1}}{\Gamma(\xi+2)}, \tag{3.31}$$

$$\mathcal{Q}_0(a,b,c)=\frac{1}{\Gamma(\xi)}\int_a^b(c-w)^{\xi-1}dw=-\frac{(c-b)^{\xi}}{\Gamma(\xi+1)}+\frac{(c-a)^{\xi}}{\Gamma(\xi+1)}. \tag{3.32}$$

By the discretization framework presented in relations (3.18) and (3.19), we construct a coupled system of equations. This system enables the numerical approximation of the unknown functions in problem (1.1) at the nodes t_{2s+1} and t_{2s+2} for $s=1,2,\ldots,\mathcal{K}-1$ that the computational procedure unfolds as follows:

$$\begin{cases}
\mathcal{S}(t_{2s+1})\simeq \mathcal{S}_0+\sigma_0^{(s)}\mathcal{F}_1^0+\sigma_1^{(s)}\mathcal{F}_1^1+\sigma_2^{(s)}\mathcal{F}_1^2+\sum_{l=1}^{s}\sigma_{2l-1}^{(s)}\mathcal{F}_1^{2l-1}+\sigma_{2l}^{(s)}\mathcal{F}_1^{2l}+\sigma_{2l+1}^{(s)}\mathcal{F}_1^{2l+1},\\
\mathcal{C}(t_{2s+1})\simeq \mathcal{C}_0+\sigma_0^{(s)}\mathcal{F}_2^0+\sigma_1^{(s)}\mathcal{F}_2^1+\sigma_2^{(s)}\mathcal{F}_2^2+\sum_{l=1}^{s}\sigma_{2l-1}^{(s)}\mathcal{F}_2^{2l-1}+\sigma_{2l}^{(s)}\mathcal{F}_2^{2l}+\sigma_{2l+1}^{(s)}\mathcal{F}_2^{2l+1},\\
\mathcal{U}(t_{2s+1})\simeq \mathcal{U}_0+\sigma_0^{(s)}\mathcal{F}_3^0+\sigma_1^{(s)}\mathcal{F}_3^1+\sigma_2^{(s)}\mathcal{F}_3^2+\sum_{l=1}^{s}\sigma_{2l-1}^{(s)}\mathcal{F}_3^{2l-1}+\sigma_{2l}^{(s)}\mathcal{F}_3^{2l}+\sigma_{2l+1}^{(s)}\mathcal{F}_3^{2l+1},\\
\mathcal{J}(t_{2s+1})\simeq \mathcal{J}_0+\sigma_0^{(s)}\mathcal{F}_4^0+\sigma_1^{(s)}\mathcal{F}_4^1+\sigma_2^{(s)}\mathcal{F}_4^2+\sum_{l=1}^{s}\sigma_{2l-1}^{(s)}\mathcal{F}_4^{2l-1}+\sigma_{2l}^{(s)}\mathcal{F}_4^{2l}+\sigma_{2l+1}^{(s)}\mathcal{F}_4^{2l+1},\\
\mathcal{H}(t_{2s+1})\simeq \mathcal{H}_0+\sigma_0^{(s)}\mathcal{F}_5^0+\sigma_1^{(s)}\mathcal{F}_5^1+\sigma_2^{(s)}\mathcal{F}_5^2+\sum_{l=1}^{s}\sigma_{2l-1}^{(s)}\mathcal{F}_5^{2l-1}+\sigma_{2l}^{(s)}\mathcal{F}_5^{2l}+\sigma_{2l+1}^{(s)}\mathcal{F}_5^{2l+1},
\end{cases} \tag{3.33}$$

and

$$\begin{cases}
\mathcal{S}(t_{2s+2})\simeq \mathcal{S}_0+\sum_{q=0}^{s}\upsilon_{2q}^{(s)}\mathcal{F}_1^{2q}+\upsilon_{2q+1}^{(s)}\mathcal{F}_1^{2q+1}+\upsilon_{2q+2}^{(s)}\mathcal{F}_1^{2q+2},\\
\mathcal{C}(t_{2s+2})\simeq \mathcal{C}_0+\sum_{q=0}^{s}\upsilon_{2q}^{(s)}\mathcal{F}_2^{2q}+\upsilon_{2q+1}^{(s)}\mathcal{F}_2^{2q+1}+\upsilon_{2q+2}^{(s)}\mathcal{F}_2^{2q+2},\\
\mathcal{U}(t_{2s+2})\simeq \mathcal{U}_0+\sum_{q=0}^{s}\upsilon_{2q}^{(s)}\mathcal{F}_3^{2q}+\upsilon_{2q+1}^{(s)}\mathcal{F}_3^{2q+1}+\upsilon_{2q+2}^{(s)}\mathcal{F}_3^{2q+2},\\
\mathcal{J}(t_{2s+2})\simeq \mathcal{J}_0+\sum_{q=0}^{s}\upsilon_{2q}^{(s)}\mathcal{F}_4^{2q}+\upsilon_{2q+1}^{(s)}\mathcal{F}_4^{2q+1}+\upsilon_{2q+2}^{(s)}\mathcal{F}_4^{2q+2},\\
\mathcal{H}(t_{2s+2})\simeq \mathcal{H}_0+\sum_{q=0}^{s}\upsilon_{2q}^{(s)}\mathcal{F}_5^{2q}+\upsilon_{2q+1}^{(s)}\mathcal{F}_5^{2q+1}+\upsilon_{2q+2}^{(s)}\mathcal{F}_5^{2q+2}.
\end{cases} \tag{3.34}$$

So, by systematically combining the governing relations (3.9), (3.14), (3.33), and (3.34), we formulate a well-posed system of $2\mathcal{K}$ equations for each unknown function. The numerical solution of this system generates discrete approximations of the unknown functions $\mathcal{S}(t)$, $\mathcal{C}(t)$, $\mathcal{U}(t)$, $\mathcal{J}(t)$ and $\mathcal{H}(t)$ at the prescribed nodal points t_j for $j=1,2,\ldots,2\mathcal{K}$.

4. Error Analysis

This section states a rigorous convergence analysis for the block-by-block discrete scheme presented.

Theorem 4.1. *Let $\mathcal{F}_k\big(t,\mathcal{S}(t),\mathcal{C}(t),\mathcal{U}(t),\mathcal{J}(t),\mathcal{H}(t)\big)\in C^3[0,T]$ for $k=1,2,3,4,5$ or in other words, the solution functions $\big\{\mathcal{S}(t),\mathcal{C}(t),\mathcal{U}(t),\mathcal{J}(t),\mathcal{H}(t)\big\}$ possess three-order continuous differentiable on the interval $[0,T]$. Then, the block-by-block numerical scheme offered in previous section converges to the exact solution with order $3+\xi$.*

Proof. Focusing first on the odd-indexed discretization steps, the local truncation error at the $(2s+1)$-th node for $s=0,1,2,\ldots,\mathcal{K}-1$ is given as

$$\begin{aligned}
\big|\mathcal{S}(t_{2s+1})-\overline{\mathcal{S}}_{2s+1}\big|\leq\frac{1}{\Gamma(\xi)}\int_0^{t_1}(t_{2s+1}-w)^{\xi-1}\Big|\Big[&\mathcal{F}_1\big(w,\mathcal{S}(w),\mathcal{C}(w),\mathcal{U}(w),\mathcal{J}(w),\mathcal{H}(w)\big)\\
&-\Big(\frac{2(w-t_{\frac{1}{2}})(w-t_1)}{\vartheta^2}\mathcal{F}_1^0+\frac{-4(w-t_0)(w-t_1)}{\vartheta^2}\mathcal{F}_1^{\frac{1}{2}}+\frac{2(w-t_0)(w-t_{\frac{1}{2}})}{\vartheta^2}\mathcal{F}_1^1\Big)\Big]
\end{aligned}$$

$$
\begin{aligned}
&+\Big(\mathcal{F}_1\big(w_{\frac{1}{2}},\mathcal{S}(w_{\frac{1}{2}}),\mathcal{C}(w_{\frac{1}{2}}),\mathcal{U}(w_{\frac{1}{2}}),\mathcal{J}(w_{\frac{1}{2}}),\mathcal{H}(w_{\frac{1}{2}})\big)\\
&-\big(\frac{3}{8}\mathcal{F}_1^0+\frac{3}{4}\mathcal{F}_1^1-\frac{1}{8}\mathcal{F}_1^2\big)\Big)\frac{-4(w-t_0)(w-t_1)}{\vartheta^2}\Big|dw\\
&+\frac{1}{\Gamma(\xi)}\sum_{l=1}^{s}\int_{t_{2l-1}}^{t_{2l+1}}(t_{2s+1}-w)^{\xi-1}\Big|\mathcal{F}_1\big(w,\mathcal{S}(w),\mathcal{C}(w),\mathcal{U}(w),\mathcal{J}(w),\mathcal{H}(w)\big)\\
&-\Big(\frac{(w-t_{2l})(w-t_{2l+1})}{2\vartheta^2}\mathcal{F}_1^{2l-1}+\frac{(w-t_{2l-1})(w-t_{2l+1})}{-\vartheta^2}\mathcal{F}_1^{2l}+\frac{(w-t_{2l})(w-t_{2l-1})}{2\vartheta^2}\mathcal{F}_1^{2l+1}\Big)\Big|dw, \qquad (4.1)\\
|\mathcal{C}(t_{2s+1})-\overline{\mathcal{C}}_{2s+1}|\le&\frac{1}{\Gamma(\xi)}\int_0^{t_1}(t_{2s+1}-w)^{\xi-1}\Big|\Big[\mathcal{F}_2\big(w,\mathcal{S}(w),\mathcal{C}(w),\mathcal{U}(w),\mathcal{J}(w),\mathcal{H}(w)\big)\\
&-\Big(\frac{2(w-t_{\frac{1}{2}})(w-t_1)}{\vartheta^2}\mathcal{F}_2^0+\frac{-4(w-t_0)(w-t_1)}{\vartheta^2}\mathcal{F}_2^{\frac{1}{2}}+\frac{2(w-t_0)(w-t_{\frac{1}{2}})}{\vartheta^2}\mathcal{F}_2^1\Big)\Big]\\
&+\Big(\mathcal{F}_2\big(w_{\frac{1}{2}},\mathcal{S}(w_{\frac{1}{2}}),\mathcal{C}(w_{\frac{1}{2}}),\mathcal{U}(w_{\frac{1}{2}}),\mathcal{J}(w_{\frac{1}{2}}),\mathcal{H}(w_{\frac{1}{2}})\big)\\
&-\big(\frac{3}{8}\mathcal{F}_2^0+\frac{3}{4}\mathcal{F}_2^1-\frac{1}{8}\mathcal{F}_2^2\big)\Big)\frac{-4(w-t_0)(w-t_1)}{\vartheta^2}\Big|dw\\
&+\frac{1}{\Gamma(\xi)}\sum_{l=1}^{s}\int_{t_{2l-1}}^{t_{2l+1}}(t_{2s+1}-w)^{\xi-1}\Big|\mathcal{F}_2\big(w,\mathcal{S}(w),\mathcal{C}(w),\mathcal{U}(w),\mathcal{J}(w),\mathcal{H}(w)\big)\\
&-\Big(\frac{(w-t_{2l})(w-t_{2l+1})}{2\vartheta^2}\mathcal{F}_2^{2l-1}+\frac{(w-t_{2l-1})(w-t_{2l+1})}{-\vartheta^2}\mathcal{F}_2^{2l}+\frac{(w-t_{2l})(w-t_{2l-1})}{2\vartheta^2}\mathcal{F}_2^{2l+1}\Big)\Big|dw, \qquad (4.2)\\
|\mathcal{U}(t_{2s+1})-\overline{\mathcal{U}}_{2s+1}|\le&\frac{1}{\Gamma(\xi)}\int_0^{t_1}(t_{2s+1}-w)^{\xi-1}\Big|\Big[\mathcal{F}_3\big(w,\mathcal{S}(w),\mathcal{C}(w),\mathcal{U}(w),\mathcal{J}(w),\mathcal{H}(w)\big)\\
&-\Big(\frac{2(w-t_{\frac{1}{2}})(w-t_1)}{\vartheta^2}\mathcal{F}_3^0+\frac{-4(w-t_0)(w-t_1)}{\vartheta^2}\mathcal{F}_3^{\frac{1}{2}}+\frac{2(w-t_0)(w-t_{\frac{1}{2}})}{\vartheta^2}\mathcal{F}_3^1\Big)\Big]\\
&+\Big(\mathcal{F}_3\big(w_{\frac{1}{2}},\mathcal{S}(w_{\frac{1}{2}}),\mathcal{C}(w_{\frac{1}{2}}),\mathcal{U}(w_{\frac{1}{2}}),\mathcal{J}(w_{\frac{1}{2}}),\mathcal{H}(w_{\frac{1}{2}})\big)\\
&-\big(\frac{3}{8}\mathcal{F}_3^0+\frac{3}{4}\mathcal{F}_3^1-\frac{1}{8}\mathcal{F}_3^2\big)\Big)\frac{-4(w-t_0)(w-t_1)}{\vartheta^2}\Big|dw\\
&+\frac{1}{\Gamma(\xi)}\sum_{l=1}^{s}\int_{t_{2l-1}}^{t_{2l+1}}(t_{2s+1}-w)^{\xi-1}\Big|\mathcal{F}_3\big(w,\mathcal{S}(w),\mathcal{C}(w),\mathcal{U}(w),\mathcal{J}(w),\mathcal{H}(w)\big)\\
&-\Big(\frac{(w-t_{2l})(w-t_{2l+1})}{2\vartheta^2}\mathcal{F}_3^{2l-1}+\frac{(w-t_{2l-1})(w-t_{2l+1})}{-\vartheta^2}\mathcal{F}_3^{2l}+\frac{(w-t_{2l})(w-t_{2l-1})}{2\vartheta^2}\mathcal{F}_3^{2l+1}\Big)\Big|dw, \qquad (4.3)
\end{aligned}
$$

and

$$
\begin{cases}
|\mathcal{J}(t_{2s+1})-\overline{\mathcal{J}}_{2s+1}| \le \dfrac{1}{\Gamma(\xi)}\displaystyle\int_0^{t_1}(t_{2s+1}-w)^{\xi-1}\Big|\Big[\mathcal{F}_4\big(w,\mathcal{S}(w),\mathcal{C}(w),\mathcal{U}(w),\mathcal{J}(w),\mathcal{H}(w)\big)\\
\quad-\Big(\dfrac{2(w-t_{\frac12})(w-t_1)}{\vartheta^2}\mathcal{F}_4^0+\dfrac{-4(w-t_0)(w-t_1)}{\vartheta^2}\mathcal{F}_4^{\frac12}+\dfrac{2(w-t_0)(w-t_{\frac12})}{\vartheta^2}\mathcal{F}_4^1\Big)\Big]\\
\quad+\Big(\mathcal{F}_4\big(w_{\frac12},\mathcal{S}(w_{\frac12}),\mathcal{C}(w_{\frac12}),\mathcal{U}(w_{\frac12}),\mathcal{J}(w_{\frac12}),\mathcal{H}(w_{\frac12})\big)\\
\quad-\big(\dfrac38\mathcal{F}_4^0+\dfrac34\mathcal{F}_4^1-\dfrac18\mathcal{F}_4^2\big)\Big)\dfrac{-4(w-t_0)(w-t_1)}{\vartheta^2}\Big|dw\\
\quad+\dfrac{1}{\Gamma(\xi)}\displaystyle\sum_{l=1}^{s}\int_{t_{2l-1}}^{t_{2l+1}}(t_{2s+1}-w)^{\xi-1}\Big|\mathcal{F}_4\big(w,\mathcal{S}(w),\mathcal{C}(w),\mathcal{U}(w),\mathcal{J}(w),\mathcal{H}(w)\big)\\
\quad-\Big(\dfrac{(w-t_{2l})(w-t_{2l+1})}{2\vartheta^2}\mathcal{F}_4^{2l-1}+\dfrac{(w-t_{2l-1})(w-t_{2l+1})}{-\vartheta^2}\mathcal{F}_4^{2l}+\dfrac{(w-t_{2l})(w-t_{2l-1})}{2\vartheta^2}\mathcal{F}_4^{2l+1}\Big)\Big|dw,\\
|\mathcal{H}(t_{2s+1})-\overline{\mathcal{H}}_{2s+1}| \le \dfrac{1}{\Gamma(\xi)}\displaystyle\int_0^{t_1}(t_{2s+1}-w)^{\xi-1}\Big|\Big[\mathcal{F}_5\big(w,\mathcal{S}(w),\mathcal{C}(w),\mathcal{U}(w),\mathcal{J}(w),\mathcal{H}(w)\big)\\
\quad-\Big(\dfrac{2(w-t_{\frac12})(w-t_1)}{\vartheta^2}\mathcal{F}_5^0+\dfrac{-4(w-t_0)(w-t_1)}{\vartheta^2}\mathcal{F}_5^{\frac12}+\dfrac{2(w-t_0)(w-t_{\frac12})}{\vartheta^2}\mathcal{F}_5^1\Big)\Big]\\
\quad+\Big(\mathcal{F}_5\big(w_{\frac12},\mathcal{S}(w_{\frac12}),\mathcal{C}(w_{\frac12}),\mathcal{U}(w_{\frac12}),\mathcal{J}(w_{\frac12}),\mathcal{H}(w_{\frac12})\big)\\
\quad-\big(\dfrac38\mathcal{F}_5^0+\dfrac34\mathcal{F}_5^1-\dfrac18\mathcal{F}_5^2\big)\Big)\dfrac{-4(w-t_0)(w-t_1)}{\vartheta^2}\Big|dw\\
\quad+\dfrac{1}{\Gamma(\xi)}\displaystyle\sum_{l=1}^{s}\int_{t_{2l-1}}^{t_{2l+1}}(t_{2s+1}-w)^{\xi-1}\Big|\mathcal{F}_5\big(w,\mathcal{S}(w),\mathcal{C}(w),\mathcal{U}(w),\mathcal{J}(w),\mathcal{H}(w)\big)\\
\quad-\Big(\dfrac{(w-t_{2l})(w-t_{2l+1})}{2\vartheta^2}\mathcal{F}_5^{2l-1}+\dfrac{(w-t_{2l-1})(w-t_{2l+1})}{-\vartheta^2}\mathcal{F}_5^{2l}+\dfrac{(w-t_{2l})(w-t_{2l-1})}{2\vartheta^2}\mathcal{F}_5^{2l+1}\Big)\Big|dw,
\end{cases}
\tag{4.4}
$$

in which $\overline{\mathcal{S}}_{2s+1}$, $\overline{\mathcal{C}}_{2s+1}$, $\overline{\mathcal{U}}_{2s+1}$, $\overline{\mathcal{J}}_{2s+1}$ and $\overline{\mathcal{H}}_{2s+1}$ are denoting the discrete approximations at the step of t_{2s+1}. Employing Taylor's theorem and Lagrange remainder, the following errors representation for $k=1,2,3,4,5$ for $\mu_1\in[0,t_1]$ and $\mu_{\frac12}\in[0,t_1]$ is established as

$$
\begin{aligned}
\big|\mathcal{R}_k^1(w)\big| &= \Big|\mathcal{F}_k\big(w,\mathcal{S}(w),\mathcal{C}(w),\mathcal{U}(w),\mathcal{J}(w),\mathcal{H}(w)\big)-\Big(\frac{2(w-t_{\frac12})(w-t_1)}{\vartheta^2}\mathcal{F}_k^0+\frac{-4(w-t_0)(w-t_1)}{\vartheta^2}\mathcal{F}_k^{\frac12}\\
&\quad+\frac{2(w-t_0)(w-t_{\frac12})}{\vartheta^2}\mathcal{F}_k^1\Big)\Big| \le \Big|\frac{\mathcal{F}_k^{(3)}\big(\mu_1,\mathcal{S}(\mu_1),\mathcal{C}(\mu_1),\mathcal{U}(\mu_1),\mathcal{J}(\mu_1),\mathcal{H}(\mu_1)\big)}{3!}(w-t_0)(w-t_{\frac12})(w-t_1)\Big|,
\end{aligned}
\tag{4.5}
$$

$$
\begin{aligned}
\big|\mathcal{R}_k^{\frac12}(w)\big| &= \Big|\mathcal{F}_k\big(w_{\frac12},\mathcal{S}(w_{\frac12}),\mathcal{C}(w_{\frac12}),\mathcal{U}(w_{\frac12}),\mathcal{J}(w_{\frac12}),\mathcal{H}(w_{\frac12})\big)-\Big(\frac38\mathcal{F}_k^0+\frac34\mathcal{F}_k^1-\frac18\mathcal{F}_k^2\Big)\Big|\\
&\le \Big|\frac{\mathcal{F}_k^{(3)}\big(\mu_{\frac12},\mathcal{S}(\mu_{\frac12}),\mathcal{C}(\mu_{\frac12}),\mathcal{U}(\mu_{\frac12}),\mathcal{J}(\mu_{\frac12}),\mathcal{H}(\mu_{\frac12})\big)}{16}\vartheta^3,
\end{aligned}
\tag{4.6}
$$

and for $l=1,2,\dots,s$ with $\mu_l\in[t_{2l-1},t_{2l+1}]$, we have

$$
\begin{aligned}
\big|\mathcal{R}_k^l(w)\big| &= \Big|\mathcal{F}_k\big(w,\mathcal{S}(w),\mathcal{C}(w),\mathcal{U}(w),\mathcal{J}(w),\mathcal{H}(w)\big)\\
&\quad-\Big(\frac{(w-t_{2l})(w-t_{2l+1})}{2\vartheta^2}\mathcal{F}_k^{2l-1}+\frac{(w-t_{2l-1})(w-t_{2l+1})}{-\vartheta^2}\mathcal{F}_k^{2l}+\frac{(w-t_{2l})(w-t_{2l-1})}{2\vartheta^2}\mathcal{F}_k^{2l+1}\Big)\Big|\\
&\le \Big|\frac{\mathcal{F}_k^{(3)}\big(\mu_l,\mathcal{S}(\mu_l),\mathcal{C}(\mu_l),\mathcal{U}(\mu_l),\mathcal{J}(\mu_l),\mathcal{H}(\mu_l)\big)}{3!}(w-t_{2l-1})(w-t_{2l})(w-t_{2l+1})\Big|.
\end{aligned}
\tag{4.7}
$$

Therefore, we derive the following principal result as:

$$\begin{cases}
|\mathcal{S}(t_{2s+1})-\overline{\mathcal{S}}_{2s+1}| \leq \frac{1}{\Gamma(\xi)}\int_0^{t_1}(t_{2s+1}-w)^{\xi-1}\left|\frac{\mathcal{M}_1}{3!}(w-t_0)(w-t_{\frac{1}{2}})(w-t_1)+\frac{\mathcal{M}_1\vartheta^3}{16}\left(\frac{-4(w-t_0)(w-t_1)}{\vartheta^2}\right)\right|dw\\
\qquad +\frac{1}{\Gamma(\xi)}\sum_{l=1}^{s}\int_{t_{2l-1}}^{t_{2l+1}}(t_{2s+1}-w)^{\xi-1}\left|\frac{\mathcal{M}_1}{3!}(w-t_{2l-1})(w-t_{2l})(w-t_{2l+1})\right|dw,\\
|\mathcal{C}(t_{2s+1})-\overline{\mathcal{C}}_{2s+1}| \leq \frac{1}{\Gamma(\xi)}\int_0^{t_1}(t_{2s+1}-w)^{\xi-1}\left|\frac{\mathcal{M}_2}{3!}(w-t_0)(w-t_{\frac{1}{2}})(w-t_1)+\frac{\mathcal{M}_2\vartheta^3}{16}\left(\frac{-4(w-t_0)(w-t_1)}{\vartheta^2}\right)\right|dw\\
\qquad +\frac{1}{\Gamma(\xi)}\sum_{l=1}^{s}\int_{t_{2l-1}}^{t_{2l+1}}(t_{2s+1}-w)^{\xi-1}\left|\frac{\mathcal{M}_2}{3!}(w-t_{2l-1})(w-t_{2l})(w-t_{2l+1})\right|dw,\\
|\mathcal{U}(t_{2s+1})-\overline{\mathcal{U}}_{2s+1}| \leq \frac{1}{\Gamma(\xi)}\int_0^{t_1}(t_{2s+1}-w)^{\xi-1}\left|\frac{\mathcal{M}_3}{3!}(w-t_0)(w-t_{\frac{1}{2}})(w-t_1)+\frac{\mathcal{M}_3\vartheta^3}{16}\left(\frac{-4(w-t_0)(w-t_1)}{\vartheta^2}\right)\right|dw\\
\qquad +\frac{1}{\Gamma(\xi)}\sum_{l=1}^{s}\int_{t_{2l-1}}^{t_{2l+1}}(t_{2s+1}-w)^{\xi-1}\left|\frac{\mathcal{M}_3}{3!}(w-t_{2l-1})(w-t_{2l})(w-t_{2l+1})\right|dw,\\
|\mathcal{J}(t_{2s+1})-\overline{\mathcal{J}}_{2s+1}| \leq \frac{1}{\Gamma(\xi)}\int_0^{t_1}(t_{2s+1}-w)^{\xi-1}\left|\frac{\mathcal{M}_4}{3!}(w-t_0)(w-t_{\frac{1}{2}})(w-t_1)+\frac{\mathcal{M}_4\vartheta^3}{16}\left(\frac{-4(w-t_0)(w-t_1)}{\vartheta^2}\right)\right|dw\\
\qquad +\frac{1}{\Gamma(\xi)}\sum_{l=1}^{s}\int_{t_{2l-1}}^{t_{2l+1}}(t_{2s+1}-w)^{\xi-1}\left|\frac{\mathcal{M}_4}{3!}(w-t_{2l-1})(w-t_{2l})(w-t_{2l+1})\right|dw,\\
|\mathcal{H}(t_{2s+1})-\overline{\mathcal{H}}_{2s+1}| \leq \frac{1}{\Gamma(\xi)}\int_0^{t_1}(t_{2s+1}-w)^{\xi-1}\left|\frac{\mathcal{M}_5}{3!}(w-t_0)(w-t_{\frac{1}{2}})(w-t_1)+\frac{\mathcal{M}_5\vartheta^3}{16}\left(\frac{-4(w-t_0)(w-t_1)}{\vartheta^2}\right)\right|dw\\
\qquad +\frac{1}{\Gamma(\xi)}\sum_{l=1}^{s}\int_{t_{2l-1}}^{t_{2l+1}}(t_{2s+1}-w)^{\xi-1}\left|\frac{\mathcal{M}_5}{3!}(w-t_{2l-1})(w-t_{2l})(w-t_{2l+1})\right|dw,
\end{cases} \tag{4.8}$$

in which $\mathcal{M}_k=\sup_{0\leq w\leq T}\left|\mathcal{F}_k^{(3)}(w,\mathcal{S}(w),\mathcal{C}(w),\mathcal{U}(w),\mathcal{J}(w),\mathcal{H}(w))\right|$ for $k=1,2,3,4,5$ and the preceding arguments demonstrate that:

$$\begin{aligned}
|\mathcal{S}(t_{2s+1})-\overline{\mathcal{S}}_{2s+1}| &\leq \frac{\mathcal{M}_1}{3!\Gamma(\xi)}\int_0^{t_1}(t_{2s+1}-w)^{\xi-1}\left|(w-t_0)(w-t_{\frac{1}{2}})(w-t_1)\right|dw\\
&+\frac{\mathcal{M}_1\vartheta^3}{16\Gamma(\xi)}\int_0^{t_1}(t_{2s+1}-w)^{\xi-1}\left|\frac{-4(w-t_0)(w-t_1)}{\vartheta^2}\right|dw\\
&+\frac{\mathcal{M}_1}{3!\Gamma(\xi)}\sum_{l=1}^{s}\int_{t_{2l-1}}^{t_{2l+1}}(t_{2s+1}-w)^{\xi-1}\left|(w-t_{2l-1})(w-t_{2l})(w-t_{2l+1})\right|dw\\
&\leq \frac{\mathcal{M}_1\vartheta^3}{3!\Gamma(\xi)}\int_0^{t_1}(t_{2s+1}-w)^{\xi-1}dw+\frac{\mathcal{M}_1\vartheta^3}{16\Gamma(\xi)}\int_0^{t_1}(t_{2s+1}-w)^{\xi-1}dw\\
&+\frac{\mathcal{M}_1\vartheta^3}{3!\Gamma(\xi)}\sum_{l=1}^{s}\int_{t_{2l-1}}^{t_{2l+1}}(t_{2s+1}-w)^{\xi-1}dw\\
&\leq \frac{\mathcal{M}_1\vartheta^{3+\xi}}{\Gamma(\xi+1)}\left((2s+1)^{\xi}-(2s)^{\xi}\right)+\frac{2^{\xi}\mathcal{M}_1\vartheta^{3+\xi}}{\Gamma(\xi)}\sum_{l=1}^{s}\left((s-l+l)^{\xi}-(s-l)^{\xi}\right)\leq \mathscr{C}_1\vartheta^{3+\xi},
\end{aligned} \tag{4.9}$$

and the preceding analysis extends to all companion functions in the system that result in:

$$\begin{cases}
|\mathcal{C}(t_{2s+1})-\overline{\mathcal{C}}_{2s+1}| \leq \mathscr{C}_2\vartheta^{3+\xi},\\
|\mathcal{U}(t_{2s+1})-\overline{\mathcal{U}}_{2s+1}| \leq \mathscr{C}_3\vartheta^{3+\xi},\\
|\mathcal{J}(t_{2s+1})-\overline{\mathcal{J}}_{2s+1}| \leq \mathscr{C}_4\vartheta^{3+\xi},\\
|\mathcal{H}(t_{2s+1})-\overline{\mathcal{H}}_{2s+1}| \leq \mathscr{C}_5\vartheta^{3+\xi},
\end{cases} \tag{4.10}$$

in which $\mathscr{C}_k$ for $k=1,2,3,4,5$ are the positive real numbers. Following the methodology established for odd-indexed temporal steps, an equivalent truncation error analysis applies to even-indexed steps and is therefore omitted for conciseness. This constructive argument verifies the theorem in full generality. □

5. Numerical experiments

This section presents the implementation and verification of the proposed multi-step numerical algorithm for solving the fractional-order financial crime model, as formulated in relation (1.1). The modified block-by-block technique is applied to solve the resulting system of nonlinear algebraic equations. To ensure computational accuracy, the discretized system of equations is resolved using the **fsolve** command, a robust numerical solver available in **Maple 18**. This approach guarantees efficient convergence while maintaining precision in the obtained solutions.

The model dynamics are determined by a set of parameters that capture the transition rates among subpopulations. In the model (1.1), we assign the following values [2, 30]: the inflow and outflow within the susceptible group is $\rho_1 = 0.12$, while the influence rate of criminals on susceptibles is $\rho_2 = 0.65$. The conversion rate of individuals to honest citizens is set as $\rho_3 = 0.05$, together with the release rate from jail $\rho_4 = 0.75$. The per capita rate of financial crime prosecution is given by $\rho_5 = 0.20$. Within the prosecution process, the discharge proportion is $\rho_6 = 0.65$, and $\rho_7 = 0.43$ reflects the discharge and acquittal rate. Finally, the rate at which prosecuted individuals are transferred to jail is $\rho_8 = 0.67$. Collectively, these parameter values embody realistic assumptions about susceptibility, recruitment, prosecution, imprisonment, and rehabilitation in the dynamics of financial crime.

$$\mathcal{S}_0 = 0.82, \quad \mathcal{C}_0 = 0.04, \quad \mathcal{U}_0 = 0.02, \quad \mathcal{J}_0 = 0, \quad \mathcal{H}_0 = 0.12. \tag{5.1}$$

Tables 1-5 present the numerical solutions obtained through the modified block-by-block scheme for $\mathcal{K} = 10$ (CPU time 10.813 s) at final time $T = 1$, with comparative benchmarks against established methods including the NDSolve numerical solver, and fourth-order Runge-Kutta (RK4) implementations for $\xi = 1$. The results demonstrate strong agreement between the proposed solutions and reference methods, validating the accuracy of our approach. To better assess the performance and compare the multi-step numerical approach and the RK4 method, the absolute error ℓ_∞ of both methods was computed using the results obtained from Mathematica's NDSolve as the reference solution. The NDSolve function, which employs adaptive step-size control and high-precision numerical techniques, provides a reliable benchmark due to its robust algorithmic foundation and certified accuracy. The absolute errors for both methods were calculated at discrete points across the computational domain and are systematically reported in Tables 1-5. The principal advantage of a block-by-block method utilizing quadratic interpolation over RK4 method is its superior computational efficiency for expensive-to-evaluate differential equations. After the initial startup phase, the block method requires only one function evaluation per step compared to four for RK4. This reduction in cost per step makes it significantly more efficient for large-scale or stiff systems where the derivative evaluation is the primary computational burden.

In the absence of an exact analytical solution, the computation of absolute error and quantitative analysis of convergence order for the rigorous assessment and computational efficacy of the algorithm's performance are evaluated by

$$\mathcal{L}_\infty(\vartheta_2) = \left|\mathcal{E}_{\vartheta_2}(T) - \mathcal{E}_{\vartheta_1}(T)\right|, \tag{5.2}$$

and

$$\mathrm{co} = \frac{\log\left(\frac{\mathcal{L}_\infty(\vartheta_1)}{\mathcal{L}_\infty(\vartheta_2)}\right)}{\log\left(\frac{\vartheta_1}{\vartheta_2}\right)}, \tag{5.3}$$

in which $\mathcal{E}_\vartheta$ denote the numerical solution corresponding to time step ϑ in terminal time T.

Table 6 - 8 provide the computed error (as defined in relation (5.2)) and corresponding convergence orders for selected values of the temporal discretization parameter ϑ, with $\xi = 1$, $\xi = 0.95$ and $\xi = 0.85$ fixed in terminal time $T = 1$. The leftmost column enumerates the ϑ values, while subsequent columns display the $\mathcal{L}_\infty$ error and experimentally determined convergence rates for the system components. The numerical results in Table 6 provide empirical validation of Theorem 4.1, demonstrating close agreement between the observed convergence rates and our theoretical predictions. In Tables 7 and 8, although this rate is robust and algebraically consistent, it does not follow the higher order predicted by Theorem 4.1 as the required conditions of the Theorem are not fully satisfied for the fractional cases of $\xi = 0.95$ and $\xi = 0.85$.

TABLE 1. Comparative numerical analysis of the solution $\mathcal{S}(t)$ for model (1.1) with $\xi = 1$ at terminal time $T = 1$.

	Presented method				
t	$\mathcal{K} = 10$	ℓ_∞	NDSolve [21]	RK4 [21]	ℓ_∞
0	0.8200000000	0	0.8200000000	0.8200000000	0
0.1	0.8159351916	1.35×10^{-09}	0.8159351930	0.8159351922	7.11×10^{-10}
0.2	0.8118831847	1.59×10^{-09}	0.8118831863	0.8118831858	5.22×10^{-10}
0.3	0.8078419766	6.73×10^{-10}	0.8078419772	0.8078419779	6.72×10^{-10}
0.4	0.8038099931	6.37×10^{-08}	0.8038099929	0.8038099946	1.70×10^{-09}
0.5	0.7997860185	6.41×10^{-10}	0.7997860179	0.7997860200	2.15×10^{-09}
0.6	0.7957691349	1.43×10^{-09}	0.7957691335	0.7957691364	2.90×10^{-09}
0.7	0.7917586714	9.79×10^{-10}	0.7917586704	0.7917586728	2.34×10^{-09}
0.8	0.7877541602	6.63×10^{-10}	0.7877541596	0.7877541614	1.87×10^{-09}
0.9	0.7837553002	5.86×10^{-10}	0.7837552997	0.7837553013	1.61×10^{-09}
1	0.7797619257	6.13×10^{-10}	0.7797619251	0.7797619266	1.42×10^{-09}

Figure 1 demonstrates the asymptotic convergence of numerical solutions to the $\xi = 1$ reference solution as $\xi \longrightarrow 1$, with observed error reduction rates confirming improved accuracy. This parametric convergence: (i) quantitatively validates the computational scheme's consistency, and (ii) empirically verifies the theoretical continuity of solutions across $0 < \xi \leq 1$.

Figure 2 shows the distribution of absolute errors at terminal times $T \in \{0.5, 1, 1.5, 2\}$ across discretization levels $\mathcal{K} = 1, 2, \ldots, 10$. The error surface plots allow direct comparison of solution precision over time. Notably, the populations (e.g., criminals and prosecuted) exhibit smooth, non-instantaneous adjustments, reflecting delayed responses characteristic of real-world systems. Fractional derivatives capture these dynamics more accurately than classical integer-order models, which often predict abrupt, less realistic changes. By incorporating historical effects, the fractional model accounts for how past prosecutions, imprisonment, and rehabilitation continue to influence current dynamics. The slower decay and longer persistence of criminal and prosecuted populations observed in Figure 2 illustrate this "memory" effect.

Figure 3 presents the computed solution over the extended domain $t \in [0, 4]$, obtained at $\mathcal{K} = 5$. The susceptible population decreases steadily as recruitment into crime (ρ_2) dominates inflow. The criminal population initially grows but later stabilizes as prosecution and rehabilitation counterbalance recruitment. Fluctuations in the prosecuted and jailed groups reflect law-enforcement dynamics, while the honest citizens compartment grows due to rehabilitation and reintegration (ρ_3 and ρ_4). Overall, the system approaches a dynamic equilibrium in which criminal activity persists but remains controlled, with rehabilitation exerting a stabilizing influence.

The integrated analysis of numerical results Tables 1-6 and visualizations Figures 1-3 provides conclusive validation of the proposed algorithm's efficacy. This multi-modal evidence demonstrates that our numerical scheme successfully resolves the target fractional-order system, and maintains consistent computational accuracy meeting theoretical error.

6. Conclusion

This research has established an innovative computational paradigm for modeling fractional-order financial crime dynamics through advanced quadratic interpolation techniques. The proposed framework demonstrates three key advancements over conventional approaches: (i) enhanced precision in capturing non-local system interactions, (ii) superior computational efficiency through optimized block decoupling, and (iii) mathematically guaranteed convergence at an accelerated rate of $\mathcal{O}(\vartheta^{3+\xi})$. Theoretical analyses and numerical validations collectively confirm the method's dual capability to maintain numerical stability while overcoming the solution coupling limitations inherent in traditional block-by-block implementations.

TABLE 2. Comparative numerical analysis of the solution $\mathcal{C}(t)$ for model (1.1) with $\xi = 1$ at terminal time $T = 1$.

	Presented method				
t	$\mathcal{K} = 10$	ℓ_∞	NDSolve [21]	RK4 [21]	ℓ_∞
0	0.0400000000	0	0.0400000000	0.0400000000	0
0.1	0.0412388722	4.17×10^{-09}	0.0412388763	0.0412388738	2.57×10^{-08}
0.2	0.0425278683	4.79×10^{-09}	0.0425278731	0.0425278711	2.04×10^{-08}
0.3	0.0438595302	2.42×10^{-09}	0.0438595327	0.0438595337	1.07×10^{-08}
0.4	0.0452275533	1.07×10^{-10}	0.0452275534	0.0452275572	3.84×10^{-08}
0.5	0.0466266276	1.05×10^{-09}	0.0466266266	0.0466266318	5.21×10^{-08}
0.6	0.0480522992	3.38×10^{-09}	0.0480522958	0.0480523034	7.54×10^{-08}
0.7	0.0495008482	2.46×10^{-09}	0.0495008457	0.0495008522	6.47×10^{-08}
0.8	0.0509691830	1.83×10^{-09}	0.0509691812	0.0509691867	5.56×10^{-08}
0.9	0.0524547479	1.46×10^{-09}	0.0524547465	0.0524547513	4.82×10^{-08}
1	0.0539554426	1.54×10^{-09}	0.0539554411	0.0539554456	4.47×10^{-08}

TABLE 3. Comparative numerical analysis of the solution $\mathcal{U}(t)$ for model (1.1) with $\xi = 1$ at terminal time $T = 1$.

	Presented method				
t	$\mathcal{K} = 10$	ℓ_∞	NDSolve [21]	RK4 [21]	ℓ_∞
0	0.0200000000	0	0.0200000000	0.0200000000	0
0.1	0.0184679080	1.05×10^{-08}	0.0184679186	0.0184679104	8.21×10^{-08}
0.2	0.0171355992	1.20×10^{-08}	0.0171356113	0.0171356033	7.97×10^{-08}
0.3	0.0159809982	7.94×10^{-09}	0.0159810061	0.0159810036	2.50×10^{-08}
0.4	0.0149844360	3.59×10^{-09}	0.0149844396	0.0149844424	2.76×10^{-08}
0.5	0.0141283939	1.31×10^{-09}	0.0141283953	0.0141284009	5.63×10^{-08}
0.6	0.0133972735	3.84×10^{-09}	0.0133972697	0.0133972808	1.11×10^{-08}
0.7	0.0127771913	2.61×10^{-09}	0.0127771887	0.0127771986	9.95×10^{-09}
0.8	0.0122557945	1.63×10^{-09}	0.0122557928	0.0122558017	8.86×10^{-09}
0.9	0.0118220961	1.40×10^{-10}	0.0118220960	0.0118221031	7.10×10^{-08}
1	0.0114663274	1.07×10^{-10}	0.0114663273	0.0114663340	6.68×10^{-09}

TABLE 4. Comparative numerical analysis of the solution $\mathcal{J}(t)$ for model (1.1) with $\xi = 1$ at terminal time $T = 1$.

	Presented method				
t	$\mathcal{K} = 10$	ℓ_∞	NDSolve [21]	RK4 [21]	ℓ_∞
0	0	0	0	0	0
0.1	0.0012323636	1.45×10^{-08}	0.0012323490	0.0012323593	1.03×10^{-08}
0.2	0.0022703591	1.68×10^{-08}	0.0022703423	0.0022703517	9.39×10^{-08}
0.3	0.0031422695	9.90×10^{-09}	0.0031422596	0.0031422599	2.82×10^{-08}
0.4	0.0038726842	2.89×10^{-09}	0.0038726813	0.0038726732	8.13×10^{-07}
0.5	0.0044829531	7.03×10^{-10}	0.0044829539	0.0044829414	1.24×10^{-08}
0.6	0.0049915866	8.35×10^{-09}	0.0049915950	0.0049915746	2.03×10^{-08}
0.7	0.0054146087	5.90×10^{-09}	0.0054146147	0.0054145969	1.77×10^{-08}
0.8	0.0057658681	4.10×10^{-09}	0.0057658723	0.0057658568	1.54×10^{-08}
0.9	0.0060573123	2.33×10^{-09}	0.0060573146	0.0060573017	1.24×10^{-08}
1	0.0062992285	2.41×10^{-09}	0.0062992309	0.0062992189	1.19×10^{-08}

TABLE 5. Comparative numerical analysis of the solution $\mathcal{H}(t)$ for model (1.1) with $\xi = 1$ at terminal time $T = 1$.

	Presented method				
t	$\mathcal{K} = 10$	ℓ_∞	NDSolve [21]	RK4 [21]	ℓ_∞
0	0.1200000000	0	0.1200000000	0.1200000000	0
0.1	0.1231256644	1.49×10^{-09}	0.1231256629	0.1231256641	1.10×10^{-09}
0.2	0.126182988	1.66×10^{-09}	0.1261829867	0.1261829871	1.14×10^{-09}
0.3	0.1291752253	1.15×10^{-09}	0.1291752241	0.1291752241	4.72×10^{-09}
0.4	0.1321053331	6.22×10^{-10}	0.1321053325	0.1321053323	1.70×10^{-09}
0.5	0.1349760066	3.45×10^{-10}	0.1349760062	0.1349760057	5.15×10^{-09}
0.6	0.1377897055	2.88×10^{-10}	0.1377897058	0.1377897046	1.17×10^{-10}
0.7	0.1405486802	1.30×10^{-10}	0.1405486803	0.1405486793	1.01×10^{-09}
0.8	0.1432549939	8.58×10^{-12}	0.1432549939	0.1432549931	8.76×10^{-09}
0.9	0.1459105432	1.71×10^{-10}	0.1459105430	0.1459105424	6.57×10^{-09}
1	0.1485170754	1.19×10^{-10}	0.1485170753	0.1485170747	5.97×10^{-09}

TABLE 6. The $\mathcal{L}_\infty$ error of the obtained results for some values of ϑ for model (1.1) with $\xi = 1$ at terminal time $T = 1$.

	$\mathcal{S}(t)$		$\mathcal{C}(t)$		$\mathcal{U}(t)$		$\mathcal{J}(t)$		$\mathcal{H}(t)$	
ϑ	$\mathcal{L}_\infty$	co	$\mathcal{L}_\infty$	co	$\mathcal{L}_\infty$	co	$\mathcal{L}_\infty$	co	$\mathcal{L}_\infty$	co
1/4	2.4283×10^{-06}	–	8.0789×10^{-06}	–	1.4983×10^{-05}	–	2.3697×10^{-05}	–	1.7928×10^{-06}	–
1/6	2.7071×10^{-07}	3.1651	7.7938×10^{-07}	3.3737	1.2769×10^{-06}	3.5525	2.1704×10^{-06}	3.4486	1.5665×10^{-07}	3.5165
1/8	5.6670×10^{-08}	3.8568	1.5776×10^{-07}	3.9397	2.4945×10^{-07}	4.0274	4.3304×10^{-07}	3.9752	3.0841×10^{-08}	4.0082
1/10	1.7237×10^{-08}	4.1370	4.7265×10^{-08}	4.1897	7.3467×10^{-08}	4.2492	1.2885×10^{-07}	4.2135	9.1181×10^{-09}	4.2358
1/12	6.6019×10^{-09}	4.3009	1.7945×10^{-08}	4.3398	2.7613×10^{-08}	4.3852	4.8726×10^{-08}	4.3579	3.4350×10^{-09}	4.3749
1/14	2.9540×10^{-09}	4.4108	7.9847×10^{-09}	4.4417	1.2203×10^{-08}	4.4785	2.1622×10^{-08}	4.4563	1.5204×10^{-09}	4.4701
1/16	1.4784×10^{-09}	4.4901	3.9805×10^{-09}	4.5158	6.0547×10^{-09}	4.5469	1.0758×10^{-08}	4.5281	7.5519×10^{-10}	4.5397
1/18	8.0524×10^{-10}	4.5503	2.1616×10^{-09}	4.5724	3.2762×10^{-09}	4.5992	5.8341×10^{-09}	4.5830	4.0897×10^{-10}	4.5930
1/20	4.6853×10^{-10}	4.5977	1.2548×10^{-09}	4.6170	1.8966×10^{-09}	4.6406	3.3831×10^{-09}	4.6263	2.3691×10^{-10}	4.6351

TABLE 7. The $\mathcal{L}_\infty$ error of the obtained results for some values of ϑ for model (1.1) with $\xi = 0.95$ at terminal time $T = 1$.

	$\mathcal{S}(t)$		$\mathcal{C}(t)$		$\mathcal{U}(t)$		$\mathcal{J}(t)$		$\mathcal{H}(t)$	
ϑ	$\mathcal{L}_\infty$	co	$\mathcal{L}_\infty$	co	$\mathcal{L}_\infty$	co	$\mathcal{L}_\infty$	co	$\mathcal{L}_\infty$	co
1/4	3.5993×10^{-06}	–	9.3408×10^{-06}	–	1.8832×10^{-05}	–	3.2300×10^{-05}	–	5.2727×10^{-07}	–
1/6	5.6765×10^{-07}	2.6646	1.1357×10^{-06}	3.0399	2.1131×10^{-06}	3.1557	4.1038×10^{-06}	2.9764	2.8736×10^{-07}	0.8756
1/8	1.6620×10^{-07}	3.0294	2.8270×10^{-07}	3.4297	5.4402×10^{-07}	3.3465	1.1203×10^{-06}	3.2019	1.2743×10^{-07}	2.0055
1/10	6.8107×10^{-08}	3.1010	1.0172×10^{-07}	3.5528	2.0643×10^{-07}	3.3682	4.4178×10^{-07}	3.2347	6.5508×10^{-08}	2.3129
1/12	3.4060×10^{-08}	3.1053	4.5698×10^{-08}	3.5862	9.7966×10^{-08}	3.3403	2.1546×10^{-07}	3.2176	3.7742×10^{-08}	2.4710
1/14	1.9385×10^{-08}	3.0913	2.3784×10^{-08}	3.5817	5.3677×10^{-08}	3.2998	1.2048×10^{-07}	3.1884	2.3631×10^{-08}	2.5678
1/16	1.2070×10^{-08}	3.0734	1.3739×10^{-08}	3.5601	3.2479×10^{-08}	3.2591	7.4036×10^{-08}	3.1587	1.5747×10^{-08}	2.6332
1/18	8.0257×10^{-09}	3.0562	8.5740×10^{-09}	3.5310	2.1122×10^{-08}	3.2222	4.8732×10^{-08}	3.1319	1.1010×10^{-08}	2.6801
1/20	5.6096×10^{-09}	3.0409	5.6778×10^{-09}	3.4994	1.4506×10^{-08}	3.1901	3.3790×10^{-08}	3.1088	7.9963×10^{-09}	2.7153

TABLE 8. The $\mathcal{L}_\infty$ error of the obtained results for some values of ϑ for model (1.1) with $\xi = 0.85$ at terminal time $T = 1$.

	$\mathcal{S}(t)$		$\mathcal{C}(t)$		$\mathcal{U}(t)$		$\mathcal{J}(t)$		$\mathcal{H}(t)$	
ϑ	$\mathcal{L}_\infty$	co	$\mathcal{L}_\infty$	co	$\mathcal{L}_\infty$	co	$\mathcal{L}_\infty$	co	$\mathcal{L}_\infty$	co
1/4	6.3852×10^{-06}	–	1.1378×10^{-05}	–	3.3084×10^{-05}	–	5.5061×10^{-05}	–	4.2130×10^{-06}	–
1/6	1.3182×10^{-06}	2.2761	1.7486×10^{-06}	2.7020	4.4004×10^{-06}	2.9104	8.8525×10^{-06}	2.6368	1.3852×10^{-06}	1.6047
1/8	4.7572×10^{-07}	2.5136	5.5083×10^{-07}	2.8490	1.4299×10^{-06}	2.7723	3.0024×10^{-06}	2.6667	5.4600×10^{-07}	2.2961
1/10	2.2281×10^{-07}	2.6365	2.3372×10^{-07}	2.9799	6.3786×10^{-07}	2.8060	1.3647×10^{-06}	2.7408	2.7029×10^{-07}	2.4440
1/12	1.2202×10^{-07}	2.6985	1.1850×10^{-07}	3.0438	3.3936×10^{-07}	2.8280	7.3373×10^{-07}	2.7809	1.5384×10^{-07}	2.5255
1/14	7.4120×10^{-08}	2.7342	6.7649×10^{-08}	3.0748	2.0218×10^{-07}	2.8404	4.4009×10^{-07}	2.8036	9.6133×10^{-08}	2.5790
1/16	4.8458×10^{-08}	2.7569	4.2019×10^{-08}	3.0892	1.3034×10^{-07}	2.8477	2.8504×10^{-07}	2.8176	6.4217×10^{-08}	2.6173
1/18	3.3465×10^{-08}	2.7723	2.7796×10^{-08}	3.0946	8.9065×10^{-08}	2.8521	1.9542×10^{-07}	2.8266	4.5102×10^{-08}	2.6460
1/20	2.4110×10^{-08}	2.7835	1.9305×10^{-08}	3.0949	6.3631×10^{-08}	2.8549	1.3998×10^{-07}	2.8328	3.2938×10^{-08}	2.6685

Future research directions include extension to stochastic fractional systems and real-time adaptive implementations for dynamic financial monitoring. The methodology's generalizability suggests potential applications in other complex socio-economic systems governed by memory-dependent dynamics.

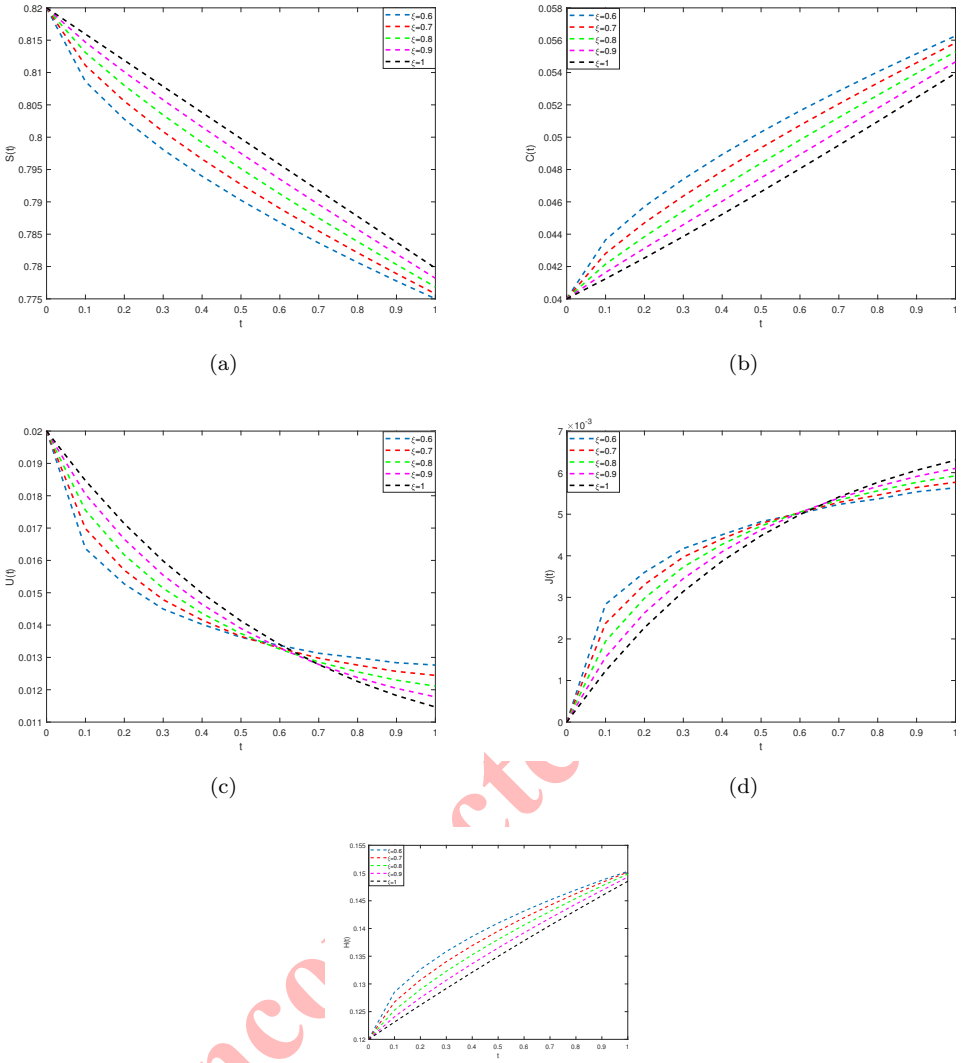

FIGURE 1. The obtained outcomes for susceptible population $\mathcal{S}(t)$ (a) criminals of financial population $\mathcal{C}(t)$ (b) under prosecution population $\mathcal{U}(t)$ (c) jailbird population $\mathcal{J}(t)$ (d) and honest people population $\mathcal{H}(t)$ for some values of ξ with $\mathcal{K} = 5$ at $T = 1$.

AVAILABILITY OF SUPPORTING DATA

The data sets generated during and/or analyzed during the current study and the code used to generate the data are available from the corresponding author upon reasonable request.

COMPETING INTERESTS

The authors declare that they have no known competing financial interests or personal relationships that could have appeared to influence the work reported in this paper.

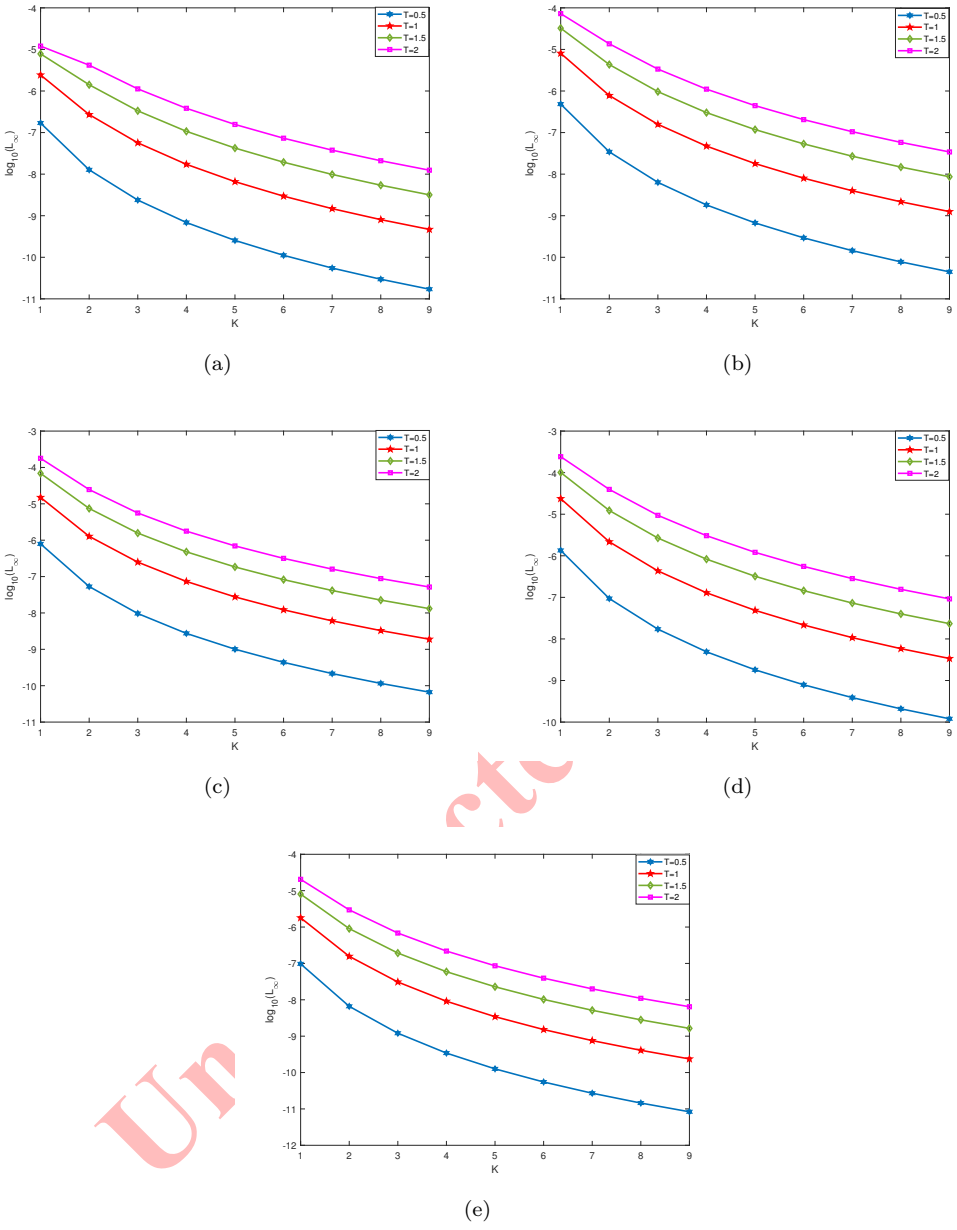

FIGURE 2. The $\mathcal{L}_\infty$ of susceptible population $\mathcal{S}(t)$ (a) criminals of financial population $\mathcal{C}(t)$ (b) under prosecution population $\mathcal{U}(t)$ (c) jailbird population $\mathcal{J}(t)$ (d) and honest people population $\mathcal{H}(t)$ for some values T and $\mathcal{K}$ with $\xi = 1$.

FUNDING

The authors received no financial support for the research, authorship, and/or publication of this article.

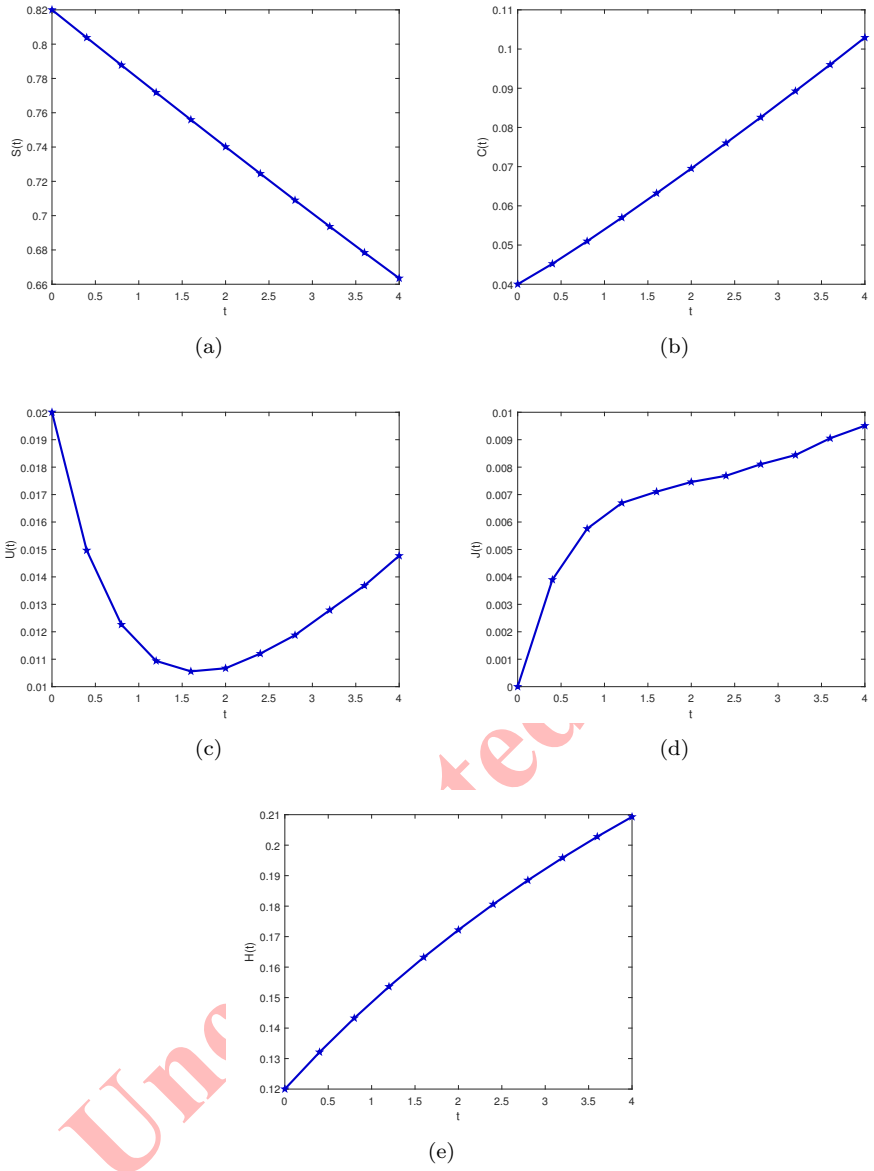

FIGURE 3. The obtained outcomes for susceptible population $\mathcal{S}(t)$ (a) criminals of financial population $\mathcal{C}(t)$ (b) under prosecution population $\mathcal{U}(t)$ (c) jailbird population $\mathcal{J}(t)$ (d) and honest people population $\mathcal{H}(t)$ for $\mathcal{K} = 5$ with $\xi = 1$ at $T = 4$.

AUTHORS' CONTRIBUTIONS

Hadis Azin, **Yadollah Ordokhani** and **Alireza Hosseinian** contributed equally to the conception, design, analysis, and writing of this manuscript.

Acknowledgments

We would like to express our sincere gratitude to all the individuals that have contributed to the publication of this research paper.

References

[1] F. Afiatdoust, M. Heydari, and M. Hosseini, *A block-by-block approach for nonlinear fractional integro-differential equations*, International Journal of Computer Mathematics, *100*(11) (2023), 2140–2155.
[2] J. Akanni, F. Akinpelu, S. Olaniyi, A. Oladipo, and A. Ogunsola, *Modelling financial crime population dynamics: optimal control and cost-effectiveness analysis*, International Journal of Dynamics and Control, *8*(2) (2020), 531–544.
[3] G. S. Becker, *Crime and punishment: An economic approach*, Journal of political economy, *76*(2) (1968), 169–217.
[4] F. Calderoni, G. M. Campedelli, A. Szekely, M. Paolucci, and G. Andrighetto, *Recruitment into organized crime: An agent-based approach testing the impact of different policies*, Journal of Quantitative Criminology, *38*(1) (2022), 197–237.
[5] D. Décary-Hétu and L. Giommoni, *Do police crackdowns disrupt drug cryptomarkets? A longitudinal analysis of the effects of Operation Onymous*, Crime, Law and Social Change, *67*(1) (2017), 55–75.
[6] P. Dellaportas, A. Alexopoulos, and O. Papaspiliopoulos, *Bayesian prediction of jumps in large panels of time series data*, Bayesian Analysis, 2022.
[7] L. M. Delves and J. L. Mohamed, *Computational methods for integral equations*, CUP Archive, 1985.
[8] V. S. Erturk and S. Momani, *Solving systems of fractional differential equations using differential transform method*, Journal of computational and Applied Mathematics, *215*(1) (2008), 142–151.
[9] J. T. Edwards, N. J. Ford, and A. C. Simpson, *The numerical solution of linear multi-term fractional differential equations: systems of equations*, Journal of Computational and Applied Mathematics, *148*(2) (2002), 401–418.
[10] C. Gerritsen and H. Elffers, *Agent-based modeling for criminological theory testing and development*, Routledge, 2020.
[11] Z. Hasan and D. S. Marisna, *Artificial Intelligence: Making crime easier in the world of finance?*, AL-ARBAH: Journal of Islamic Finance and Banking, *6*(2) (2024), 223–256.
[12] J. Huang, Y. Tang, and L. Vázquez, *Convergence analysis of a block-by-block method for fractional differential equations*, Numerical Mathematics: Theory, Methods and Applications, *5*(2) (2012), 229–241.
[13] M. Jofre, A. Bosisio, and M. Riccardi, *Financial crime risk assessment: machine learning insights into ownership structures in secrecy firms*, Global Crime, *25*(3-4) (2024), 242–267.
[14] R. Katani and S. Shahmorad, *Block by block method for the systems of nonlinear volterra integral equations*, Applied Mathematical Modelling, *34*(2) (2010), 400–406.
[15] R. Katani and S. Shahmorad, *A block by block method for solving system of volterra integral equations with continuous and abel kernels*, Mathematical Modelling and Analysis, *20*(6) (2015), 737–753.
[16] R. Katani, S. Shahmorad, and D. Conte, *Approximate solution of multi-term fractional differential equations via a block-by-block method*, Journal of Computational and Applied Mathematics, *453* (2025), 116135.
[17] M. M. Khader, N. H. Sweilam, and A. M. Mahdy, *Two computational algorithms for the numerical solution for system of fractional differential equations*, Arab Journal of Mathematical Sciences, *21*(1) (2015), 39–52.
[18] P. Kumar and O. P. Agrawal, *An approximate method for numerical solution of fractional differential equations*, Signal processing, *86*(10) (2006), 2602–2610.
[19] M. Levi, *Financial crimes-a criminological research perspective*, Edward Elgar Publishing, 2022.
[20] P. Linz, *Analytical and numerical methods for Volterra equations*, SIAM, 1985.
[21] G. Manohara and S. Kumbinarasaiah, *A study of fractional order financial crime model using the gegenbauer wavelet collocation method*, Advanced Theory and Simulations, *8*(3) (2024), 2400998.
[22] F. Mirzaee and Z. Rafei, *The block by block method for the numerical solution of the nonlinear two-dimensional Volterra integral equations*, Journal of King Saud University-Science, *23*(2) (2011), 191–195.
[23] S. Momani and K. Al-Khaled, *Numerical solutions for systems of fractional differential equations by the decomposition method*, Applied Mathematics and Computation, *162*(3) (2005), 1351–1365.

[24] C. Morselli, *Contacts, opportunities, and criminal enterprise*, University of Toronto Press, 2005.
[25] I. Podlubny, *Fractional differential equations: an introduction to fractional derivatives, fractional differential equations, to methods of their solution and some of their applications*, Elsevier, 1998.
[26] A. Rahman, P. Debnath, A. Ahmed, H. M. Dalim, M. Karmakar, M. F. I. Sumon, and M. Khan, *Machine learning and network analysis for financial crime detection: Mapping and identifying illicit transaction patterns in global black money transactions*, Gulf Journal of Advance Business Research, *2*(6) (2024), 250–272.
[27] P. Reuter and M. A. Kleiman, *Risks and prices: An economic analysis of drug enforcement*, Crime and justice, *7* (1986), 289–340.
[28] J. Saberi-Nadjafi and M. Heidari, *A generalized block-by-block method for solving linear Volterra integral equations*, Applied mathematics and computation, *188*(2) (2007), 1969–1974.
[29] A. Young, *The application of approximate product-integration to the numerical solution of integral equations*, Proceedings of the Royal Society of London. Series A. Mathematical and Physical Sciences, *224*(1159) (1954), 561–573.
[30] R. Zarin, A. Raouf, A. Khan, A. A. Raezah, and U. Wannasingha, *Computational modeling of financial crime population dynamics under different fractional operators*, AIMS Mathematics, *8*(9) (2023), 20755–20789.
[31] M. Zhang, X. Yang, and Y. Cao, *Numerical analysis of block-by-block method for a class of fractional relaxation-oscillation equations*, Applied Numerical Mathematics, *176* (2022), 38–55.